

Yeast growth is controlled by the proportional scaling of mRNA and ribosome concentrations

Xin Gao¹, Michael Lanz^{1,2}, Rosslyn Grosely³, Jonas Cremer¹, Joseph Puglisi³, and Jan M. Skotheim^{1,2,*}

¹Department of Biology, Stanford University, Stanford, California, USA

²Chan Zuckerberg Biohub, San Francisco, California, USA

³Department of Structural Biology, Stanford University School of Medicine, Stanford, California, USA

*Address correspondence to skotheim@stanford.edu

ABSTRACT

Despite growth being fundamental to all aspects of cell biology, we do not yet know its organizing principles in eukaryotic cells. Classic models derived from the bacteria *E. coli* posit that protein-synthesis rates are set by mass-action collisions between charged tRNAs produced by metabolic enzymes and mRNA-bound ribosomes. These models show that faster growth is achieved by simultaneously raising both ribosome content and peptide elongation speed. Here, we test if these models are valid for eukaryotes by combining single-molecule tracking, spike-in RNA sequencing, and proteomics in 15 carbon- and nitrogen-limited conditions using the budding yeast *S. cerevisiae*.

Ribosome concentration increases linearly with growth rate, as in bacteria, but the peptide elongation speed remains constant (≈ 9 amino acids s^{-1}) and charged tRNAs are not limiting. Total mRNA concentration rises in direct proportion to ribosomes, driven by enhanced RNA polymerase II occupancy of the genome. We show that a simple kinetic model of mRNA–ribosome binding predicts both the fraction of active ribosomes, the growth rate, and responses to transcriptional perturbations. Yeast accelerate growth by coordinately and proportionally co-up-regulating total mRNA and ribosome concentrations, not by speeding elongation. Taken together, our work establishes a new framework for eukaryotic growth control and resource allocation.

INTRODUCTION

Cells continuously tune their biosynthetic capacity in response to nutrient availability. A hallmark of this coordination is the increase in ribosome abundance as growth accelerates, which has been observed in diverse species including bacteria and yeast^{1–8}. Elegant quantitative models developed for the bacteria *E. coli* describe growth as a mass-action process in which charged tRNAs collide with mRNA-bound ribosomes^{9–13}. By balancing the proteome fractions devoted to metabolism (which supplies charged tRNAs) and translation (ribosomes which consume them), these models predict how ribosome content, active-ribosome fraction, and peptide-elongation rate change with growth rate. While these quantitative models developed for *E. coli* have proven useful, there is little in these models that is specific to bacterial physiology. This raises the question whether the same principles apply to eukaryotes¹⁴. Here, inspired by models of bacterial growth physiology, we aim to identify the fundamental principles governing eukaryotic growth by examining the budding yeast *S. cerevisiae*.

In *S. cerevisiae*, it is currently unclear which molecular components are limiting for cell growth. Proteome surveys report that ribosome content rises with growth rate^{1,3–7}, but indirect proxies such as polysome profiles suggest that a sizable fraction of ribosomes may remain inactive^{4,15}, and average translation rates for a ribosome have been reported to either increase or remain constant with growth rate^{15–21}. Moreover, ribosomes are not the only expensive biosynthetic investment and metabolic enzymes, tRNAs, or mRNAs could also limit growth. In *E. coli*, mRNA concentrations increase when cells grow faster^{10,11,22}, but it is unclear whether yeast behave similarly because the scaling of the total mRNA concentration with growth rate has never been measured directly^{23–25}.

Here, we measure every variable needed to construct a model of eukaryotic cell growth. Single-molecule tracking of Halo-tagged ribosomal proteins quantifies the fraction of actively translating ribosomes across 15 carbon- and nitrogen-limited conditions, while spike-in RNA-seq, tRNA RT-qPCR, and quantitative proteomics yield absolute mRNA, tRNA, and ribosome concentrations, respectively. We find that (i) the active ribosome fraction increases with growth rate; (ii) the peptide-elongation rate stays essentially constant at ~ 9 aa s⁻¹; and (iii) the total mRNA concentration increases in proportion to the growth rate. These patterns contradict canonical bacterial models but align with a new kinetic framework in which mRNA-ribosome mass-action kinetics, rather than charged tRNA, limits protein synthesis. Yeast therefore accelerates growth by up-regulating both ribosomes and mRNA, which establishes a new quantitative paradigm for eukaryotic growth physiology.

RESULTS

To determine how yeast grow at different rates in different environments, we sought to measure the compositional changes of the major building blocks of biosynthesis, including ribosomes, tRNA, and mRNA. To do this, we started by measuring ribosome concentrations. We grew *S. cerevisiae* strains on 15 different media (12 carbon sources and 3 different nitrogen sources) and performed mass spectrometry (see **Methods**). Consistent with previous results^{3–7}, we found a linear increase in the fraction of the proteome devoted to ribosomal proteins as the growth rate increases (**Fig. 1a**; **Extended Data Fig. 1a**).

The fraction of actively translating ribosomes increases with growth rate

That the concentration of ribosomes increases linearly with the growth rate suggests that this is the limiting factor for growth, *i.e.*, more ribosomes drive proportionally faster growth. However, some work suggested that there may be a pool of inactive ribosomes that complicates this simple model^{4,15}. This hypothesis was supported by a recent study that estimated the fraction of active ribosomes using polysome profiling under two growth conditions⁴. However, polysome profiles are difficult to quantify and treating the proportion of polysomes as a proxy for the fraction of active ribosomes may be problematic because monosomes could also contribute to translation^{26,27}. We therefore sought an alternative method to directly measure the active ribosome fraction in a variety of growth conditions.

During peptide elongation, ribosomes bound to mRNA are characterized by a slow diffusion coefficient due to the large size of mRNA, whereas inactive ribosomes diffuse freely in the cytoplasm and exhibit a high diffusion coefficient²⁸. To calculate the diffusion coefficient of ribosomes and then quantify the active ribosome fraction in living yeast cells, we employed single-molecule tracking²⁹ (**Fig. 1b**). To track individual ribosomes in living yeast, we first deleted the membrane transporter gene *PDR5* to retain fluorescent dyes inside the cells. We then fused the Halo tag to the C-terminus of the ribosomal subunits Rps4b, Rps9a, Rpl26a, and Rpl29³⁰. Among these, *RPS9A-Halo* and *RPL26A-Halo* strains maintain growth rates similar to wild-type (**Extended Data Fig. 1b-d**). We therefore decided to use the strain expressing *RPS9A-Halo* for further analysis. Briefly, cells were labeled with the PA549 dye before we performed live-cell photoactivated localization microscopy (PALM) for over 50 cells for each condition (**Fig 1c**; **Extended Data Fig. 1e**; see **Methods**). The diffusion coefficient of a single ribosome D_a can be calculated from the stepwise mean-squared displacement (MSD) of its trajectory. To determine the active ribosome fraction, we fit the distribution of ribosome diffusion coefficients in a population using a Gaussian mixture model

composed of a slow-diffusing active fraction and a fast-diffusing inactive fraction (**Fig. 1d**).

To validate our approach, we treated cells with the translation initiation inhibitor lactimidomycin (LMT), which stalls ribosomes at the start codon and allows already elongating ribosomes to run off the mRNA. In glucose-grown cells, LMT treatment reduced the fraction of slowly diffusing ribosomes from 70% to 35% (**Fig. 1e**). Our data are consistent with the observation that mRNA concentration is approximately one-third that of the ribosome concentration^{31,32}. This is because in our experiment, we expect that sometime after LMT treatment, the actively translating ribosomes would all have run off their mRNA. There would also be sufficient time for unbound ribosomes to be loaded onto the start codon of each mRNA, where it would stall so that each mRNA would then be bound to a single ribosome. These results suggest that our single-molecule tracking-based method accurately reflects the fraction of active ribosomes bound to mRNA.

After establishing our method to measure the active ribosome fraction, we sought to determine how this fraction changes in different growth conditions. To do this, we examined yeast cells growing in 12 different carbon sources and 3 different nitrogen-limited conditions³³ (**Fig. 1f**; **Extended Data Fig. 1f**). The average diffusion coefficients were similar across all these growth conditions and consistent with theoretical estimates using the Stokes-Einstein equation applied to a typical 80S monosome or a 40S ribosome subunit^{34,35} (**Fig. 1g**; **Extended Data Fig. 1g**). Moreover, our results indicate that the active ribosome fraction is positively correlated with growth rate (**Fig. 1h**). The slower cells grow, the larger the fraction of inactive ribosomes. To confirm this observation, we repeated these experiments with a strain expressing *RPL26A-Halo* to label the 60S ribosomal subunit, which can remain associated with the endoplasmic reticulum (ER) after the translation of some proteins³⁶. Diffusion measurements of *RPL26A-Halo* revealed a similar increase in the active ribosome fraction with growth rate as for the 40S subunit (**Extended Data Fig. 2a-b**). We note that our estimates of the active fraction may be slightly large due to some ribosomes being associated with compartments like the ER, which can reduce their mobility even if they are not actively translating^{37,38}. To confirm our results, we therefore performed polysome profiling on cells grown in four conditions. The polysome percentage rose at higher growth rates, while the 40S and 60S peaks declined, reflecting a higher proportion of ribosomes in an active state (**Fig. 1i**; **Extended Data Fig. 2c**).

Thus, we find that the fraction of the proteome that is active ribosomes increases in proportion to the growth rate, while the fraction of the proteome that is inactive ribosomes is slightly decreased from 10% to 8% (**Fig. 1j**). In other words, as yeast grow faster, they engage proportionally more ribosomes in translation while there remains a substantial inactive fraction of ribosomes.

Global peptide elongation rate is independent of growth rate

After estimating the active ribosome fraction, we can now estimate the average peptide elongation rate of a translating ribosome, a predicted output of several growth models. We neglect protein degradation in our analysis because the vast majority of the proteome is stable on the time scale of a cell division cycle^{39,40}. The peptide elongation rate, c_p , is related to the average protein mass per cell, m_{prot} , the active ribosomes per cell N_{ribo}^{active} , the population doubling time T_d by the following equation¹⁹:

$$c_p = \frac{m_{prot} \ln 2}{N_{ribo}^{active} T_d}.$$

If the ribosome fraction in the proteome is ϕ_r , the fraction of ribosomes that is active is ϕ_a , and the average protein mass of a single ribosome is m_{rb} , then the average ribosomal protein mass in a cell is

$$m_{prot} \phi_r = N_{ribo} m_{rb} = \frac{N_{ribo}^{active} m_{rb}}{\phi_a}.$$

Substituting m_{prot} in the equation for the peptide elongation rate yields:

$$c_p = \frac{m_{rb} \ln 2}{\phi_a \phi_r T_d}.$$

Examining the peptide elongation rate in different growth conditions revealed that it is nearly independent of growth rate (~9 amino acids per second; **Fig 2a**). In contrast, previous studies estimated elongation rates assuming that all ribosomes were active. If we make this erroneous assumption, the average elongation rate increases with growth rate, consistent with earlier reports^{15,16,18–20,41} (**Extended Data Fig. 3a**). In addition, we examined whether translation efficiencies (ribosome footprints/mRNA reads for a given gene, see **Methods**) change with growth rate^{42,43}. By combining ribosome footprints and RNA-seq, we found that translation efficiencies across genes span approximately two orders of magnitude. Despite the large-scale remodeling of the transcriptome in different carbon sources, the translation efficiency of individual genes remained largely stable across conditions (**Extended Data Fig. 3b-d**).

To validate our method for calculating peptide elongation rates, we treated yeast cells growing in four different carbon sources with the translation inhibitor cycloheximide (CHX). CHX treatment decreased the growth rate in all conditions. Compared to untreated cells, CHX-treated cells exhibited significant proteomic alterations, including

to the ribosome concentration we need to calculate the peptide elongation rate (**Fig. 2b; Extended Data Fig. 3e**). The peptide elongation rate in CHX-treated cells was significantly reduced, consistent with expectations (**Fig. 2c; Extended Data Fig. 3f**). To further test the notion that the average peptide elongation rate was similar across conditions, we compared the onset of luminescence from reporters containing variable-length coding sequences inserted upstream of the *Nluc* luciferase gene in two different growth conditions^{17,44}. Consistent with our other data, we observed no significant differences in the luciferase onset time in the two growth conditions (**Extended Data Fig. 3g-h**).

That the average peptide elongation rate is constant across growth conditions distinguishes *S. cerevisiae* from the bacteria *E. coli*, where the peptide elongation rate increases with increasing growth rate from 8 to 16 aa/s^{10,14}.

tRNA is in excess in fast growth condition

To explore why the peptide elongation rate is constant across growth conditions, we examined how translation machinery components vary with the growth rate. We first quantified tRNA concentrations under five conditions by RT-qPCR, relative to three housekeeping genes with stable mRNA concentration across all five tested conditions⁴⁵. Almost all nuclear-encoded tRNA increases concentration with increasing growth rate and is proportional to the concentration of active ribosomes (**Fig. 2d; Extended Data Fig. 4a-b**). Translation-related proteins all increase in concentration with increasing growth rate, but the elongation factors eEF1A, eEF1B, eEF2, and several initiation factors may increase in concentration more slowly than eEF3 and tRNA synthetases (**Fig. 2e; Extended Data Fig. 4c**).

That the peptide elongation rate remains constant suggests that charged tRNA are in excess and not limiting for growth. In other words, reducing the concentration of charged tRNA complexes should initially not impact cell growth. We sought to test this hypothesis by modulating the concentration of available charged tRNA. To do this, we manipulated eEF1A expression by deleting *TEF2* and replacing the promoter of *TEF1* with an aTc-inducible P_{tet} promoter⁴⁶ (**Fig. 2f**). Reduction of available eEF1A reduces the export of tRNA from the nucleus, and thereby reduces the available charged tRNA for elongating ribosomes^{47–49}. We expect that this manipulation should reduce the concentration of charged tRNA-eEF1A complexes in the cytoplasm because in glucose ~90% of the tRNAs are charged⁵⁰. Remarkably, reducing eEF1A levels to 30% of the original level did not affect growth rate, the fraction of active ribosomes, or the peptide elongation rate (**Fig. 2g and Extended Data Fig. 4d-e**). Further reduction of eEF1A is lethal and we were unable to measure any intermediate states. Taken together, these experiments suggest that tRNA-complex availability is in excess in nutrient-rich

environments so that even when they are reduced in slower growth conditions, the peptide elongation rates remain unaffected.

Global mRNA concentration increases with growth rate

While most previous experimental studies of cell growth have focused on ribosomes as being limiting, theoretical work shows it is also possible for mRNA to be limiting ²². Indeed, proteomic analysis revealed that the proteins exhibiting the most significant differences across growth conditions were primarily associated with both ribosomes and mRNA synthesis (**Extended Data Fig. 5a**). To test if growth rates drove changes in mRNA concentration, we performed spike-in RNA sequencing on yeast grown in four carbon sources with distinct growth rates. This showed that the total mRNA concentration increases monotonically with the growth rate (**Fig. 3a; Extended Data Fig. 5b-e**). In contrast, global protein concentrations were similar across the 4 conditions (**Extended Data Fig. 5f**). For each gene, we observed that the protein fraction was close to proportional to the corresponding mRNA fraction across the conditions even though the global mRNA concentration changes (**Fig. 3b; Extended Data Fig. 5g**). This suggests a picture in which a global protein concentration is maintained and that the relative concentrations of specific proteins is largely determined by their relative mRNA concentrations ⁵¹. Taken together, our data suggest that global mRNA concentrations increase with growth rate in *S. cerevisiae* similar to what was found for bacteria ¹⁰.

Mass action kinetics of RNAP II and the genome may explain growth-dependent increases in mRNA concentrations

To explore why mRNA concentration increases with growth rate, we first examined the concentrations of RNA polymerase II (RNAP II) subunits and their corresponding mRNA and found that they all slightly increased with the growth rate (**Fig. 3c and Extended Data Fig. 6a-b**). Since mRNA concentrations result from the balance of synthesis and degradation, we sought to determine whether mRNA decay rates varied across carbon sources. To do this, we acutely repressed the transcription of the methionine regulated genes *MET3* and *MET17* and measured their mRNA concentrations by RT-qPCR (see **Methods**). mRNA decay rates were nearly the same in all tested conditions (**Fig. 3d and Extended Data Fig. 6c**). Therefore, we suggest that the increase in mRNA concentration with growth rate is primarily driven by increases in transcription rather than degradation.

To understand more precisely how increasing RNAP II concentrations could drive increasing mRNA concentrations, we built a mathematical model (**Fig. 3e**). In our

model, the concentration of DNA-bound RNAP II, $[pol_{bound}]$, is determined by mass action kinetics of free RNAP II, $[pol_{free}]$, and the genome. Dissociation of the DNA-bound RNAP II is modeled using first order kinetics with off-rate k_{off}^{pol} so that:

$$\frac{d[pol_{bound}]}{dt} = k_{on}^{pol}[DNA][pol_{free}] - k_{off}^{pol}[pol_{bound}] \text{ and}$$

$$[pol_{total}] = [pol_{free}] + [pol_{bound}] = \frac{P\phi_{pol}}{f},$$

where P is the global protein concentration, ϕ_{pol} is the RNAP II fraction in proteome and $f = V_{nucleus}/V_{cell}$ denotes the ratio of nuclear volumes $V_{nucleus}$ to cell volumes V_{cell} . At steady-state, these two equations can be solved for the fraction of RNAP II that is DNA-bound:

$$\frac{[pol_{bound}]}{[pol_{total}]} = \frac{1}{1 + \frac{K_d^{pol}}{[DNA]}} = \frac{1}{1 + \frac{K_d^{pol}V_{cell}f}{DNA}},$$

where $K_d^{pol} = k_{off}^{pol}/k_{on}^{pol}$ is the dissociation constant of RNAP II. mRNA is produced by bound RNAP II in the nucleus and then exported to the cytoplasm so that

$$\frac{d[mRNA]}{dt} = k_{trans}^{mRNA}[pol_{bound}]f - k_d^{mRNA}[mRNA],$$

where k_{trans}^{mRNA} is the mRNA transcription rate and k_d^{mRNA} is the average degradation rate. At steady state, we can solve these equations for the mRNA concentration to yield:

$$[mRNA] = \frac{k_{trans}^{mRNA}}{k_d^{mRNA}} [pol_{total}] \phi_{pol}^{bound} f = \frac{k_{trans}^{mRNA} P \phi_{pol}}{k_d^{mRNA} \left(1 + \frac{K_d^{pol} V_{cell} f}{DNA} \right)}.$$

We independently measured the global protein concentration, RNAP II fraction in proteome, DNA content, cell and nuclear volumes, and mRNA decay rate for 4 growth conditions. To measure the nuclear volume fraction f for each condition, we used Pus1-eGFP as a nuclear marker. f changes significantly depending on the growth condition, which impacts the nuclear concentrations of the genome and RNAP II (**Fig. 3f-g and Extended Data Fig. 6d-e**). We further experimentally determined the fraction of DNA-bound RNAPII using single-molecule tracking of the largest subunit, *RPB1-Halo* using methods we previously established²⁵. DNA-bound RNAP II shows a slow

diffusion coefficient, while free RNAPII diffuses rapidly. In glucose, approximately 58% of RNAPII is bound to DNA, consistent with previous reports^{25,52}. In slow growth conditions, the fraction of DNA-bound RNAPII decreases to 30% (**Fig. 3h and Extended Data Fig. 6f**).

Our measurements greatly constrain our model so that we are left with only one free parameter, K_d^{pol} , to fit the fraction of RNAP II that is DNA bound. mRNA concentrations are then scaled with a second free parameter, the mRNA transcription rate k_{trans}^{mRNA} . Our two fit parameters are the same for all 4 growth conditions. Our simple transcription model recapitulates the observed increase in the fraction of DNA-bound RNAPII with growth rate and increasing mRNA concentrations (**Fig. 3i-j**). Our simple model assumes that transcription dynamics are the same in all these conditions and that the total amount of transcription is due to mass action kinetics of free nuclear RNAP II and the genome. This model is similar to the one we previously used to explain how the total amount of transcripts scaled in proportion to the cell volume in a given growth condition²⁵.

Mass action kinetics of free ribosomes and mRNA determine cellular growth

Since both mRNA and ribosome concentrations increase with growth rate, we hypothesize that mRNA–ribosome association and initiation kinetics may determine the fraction of active ribosomes and thereby determine the cellular growth rate. To test this hypothesis, we developed a dynamic equilibrium model describing mRNA-ribosome association and dissociation with mass action kinetics and first order decay, respectively (**Fig. 4a**). During translation initiation, the small ribosomal subunit binds near the 5'-end of the mRNA, scans to the start codon, and recruits the large subunit to form the complete 80S ribosome⁵³. For simplicity, our model treats the 80S ribosome as a single unit that binds to an mRNA binding site, undergoes translation initiation, and then elongation. The ribosome then dissociates upon completion of translation and recycles back into the free pool. Assuming that elongating ribosomes do not saturate the mRNA, the concentration of ribosomes sitting in the initiating position, $[ribo_{init}]$, is determined by the concentration of free ribosomes, $[ribo_{free}]$, the free ribosome binding sites on the mRNA, $[RBS_{free}]$, the associated binding rate, k_{on}^{ribo} , and the rate of initiating translation, k_{init}^{ribo} , so that:

$$\frac{d[ribo_{init}]}{dt} = k_{on}^{ribo} [RBS_{free}] [ribo_{free}] - k_{init}^{ribo} [ribo_{init}].$$

After initiation, ribosomes form part of a translating pool whose concentration $[ribo_{trans}]$ is determined by the initiation rate and the termination rate, k_{off}^{ribo} , so that:

$$\frac{d[ribo_{trans}]}{dt} = k_{init}^{ribo}[ribo_{init}] - k_{off}^{ribo}[ribo_{trans}].$$

In addition, we can write the total ribosome concentration, $[ribo_{total}]$, as the sum of the distinct pools of ribosomes so that

$$[ribo_{total}] = [ribo_{free}] + [ribo_{init}] + [ribo_{trans}].$$

Finally, we use the fact that the mRNA concentration equals to concentration of free ribosome binding sites (only one per mRNA) and concentration of occupied ribosome binding sites:

$$[mRNA_{total}] = [ribo_{init}] + [RBS_{free}].$$

We then scale our variables to make the equations dimensionless and solve them for steady state solutions (see **Methods** and **Extended Data Fig. 7a**). This results in a set of equations with a single free parameter, α_{glc} , which is the dimensionless mRNA concentration in glucose. Using our single free parameter, we fit our data for the active ribosome fraction as a function of the cellular growth rate in all our conditions (**Fig. 4b**; **Extended data Fig. 7b-c**). Taken together, our analysis shows that the fraction of active ribosomes could be determined by simple mass action kinetics (**Fig. 4c**).

To directly test our model that the fraction of active ribosomes is determined by mRNA and ribosome mass action kinetics, we sought to reduce the mRNA concentration. To do this, we again used the anhydrotetracycline (aTc)-inducible promoter⁴⁶ to control the expression of the RNAP II subunit *RPB1* so that it ranges from negligible amounts to above the wild type level (**Extended Data Fig. 7d**). This yeast strain cannot survive without aTc, and its growth rate increases with aTc dosage, reaching a maximum at approximately 30 ng/mL (**Extended Data Fig. 7e**). Spike-in mRNA sequencing showed that global mRNA concentrations rose from 0.4-fold to near-normal levels as aTc dosage increased (**Fig. 4d**). Lowering mRNA concentrations reduced the fraction of active ribosomes as predicted by our model (**Fig. 4d and Extended Data Fig. 7f**).

Yeast cells coordinate mRNA and ribosomes to regulate growth rate

Our model is easily extended to predict the growth rate, λ , which is proportional to the concentration of active ribosomes since the peptide elongation rate is constant across different conditions:

$$\lambda = \frac{c_p \phi_a \phi_r}{m_{rb}} .$$

Thus, for the four conditions where we have measured all the model's parameters, we agree with our experimental results (**Fig. 4e**). In principle, the growth rate can be increased by either increasing any combination of the mRNA or ribosome concentrations. However, *S. cerevisiae* appears to coordinate this regulation so that the ribosome to mRNA ratio is constant (**Fig. 4f**).

We further tested our growth model by examining a naturally occurring situation where the mRNA concentration decreases, but the ribosome concentration remains constant. This occurs when yeast cells are arrested in the G1 phase of the cell cycle for extended periods of time^{25,54} (**Extended Data Fig. 7g**). In this case, we accurately predict how the growth rate declines with the decreasing mRNA concentration (**Fig. 4g**; **Extended Data Fig. 7h-i**).

DISCUSSION

Our measurements reveal that budding yeast modulates growth by coordinately increasing both ribosome and mRNA concentrations, thereby raising the fraction and absolute number of active ribosomes that translate at a constant elongation speed. This strategy contrasts with bacterial paradigms, where growth is tuned by both the ribosome supply and charged-tRNA that accelerates elongation speed. In yeast, charged tRNAs appear buffered to maintain a constant elongation speed. Instead, mass-action kinetics between mRNA and ribosomes sets the growth rate. These findings establish a new quantitative framework for eukaryotic growth in which it is determined both by global transcriptional output and ribosome biogenesis.

Mechanistically, our framework rests on two simple mass action kinetic models (**Fig. 4h**). First, RNAP II concentration increases with the growth rate to increase its rate of association with the genome. This drives a proportional increase in the concentration of total mRNA. Second, ribosome biogenesis increases in proportion to the growth rate so that the active fraction of ribosomes is determined by mass action kinetics with mRNA. As mRNA and ribosome pools rise in lock-step, the concentration of active ribosomes increases to determine the growth rate.

These results have unexpected evolutionary implications. First, since charged-tRNA are buffered, it should be possible to increase the growth rate by increasing either the ribosome concentration or the mRNA concentration, even in rich nutrient conditions such as glucose containing media. That yeast does not do so, after decades of propagation in the laboratory, suggests that laboratory conditions represent a more complex ecology than is generally thought. Consistent with this notion, evolution

experiments are quickly able to select for more fit mutants in specific environments ^{55,56}. Second, to increase growth rate, yeast coordinately upregulate both ribosome and mRNA concentrations. It is not obvious why it does so because the most efficient way would be to simply increase mRNA, which is 1-2% of the cell's dry mass, rather than ribosomes, which are over 10%. Thus, while it is possible to produce a particular growth rate with a continuous range of ribosome and mRNA concentrations, yeast appear to be constrained to maintain about 2 ribosomes per mRNA.

While the mechanistic reason for the coordinated regulation of mRNA and ribosomes can be understood as being due to both ribosome biogenesis and RNAP II synthesis being downstream of a common mTOR activity ^{57,58}, the evolutionary reasons for this apparent constraint are currently a mystery. One possibility is that the regulation of eukaryotic growth will be better understood when we consider dynamic environments requiring rapid adaptation. While mRNA concentrations can be rapidly tuned on a 10-minute timescale, ribosome concentrations can only slowly be tuned on a timescale of hours. It could be possible that maintaining a higher concentration of ribosomes better prepares the cell to take advantage of rapid upshifts in nutrients, while making growth also dependent on the quickly turned over mRNA allows the cell to quickly respond to worsening conditions. Certainly, more work needs to be done to understand how growth, perhaps the most fundamental physiological property of a cell, is coordinated in response to environmental conditions. While our work is an important step forward in this path, we anticipate future work extending our single-molecule tracking and spike-in transcriptomic methods to other eukaryotic cells to test the generality of our framework and refine models of cellular growth.

Acknowledgements

ZY478 and ZY483 are gifts from the Zid lab. This work was supported by the National Institute of Health R35 GM134858. We thank Huan Zheng, Skye Glenn, and Cristhian Chumplitaz for teaching us the single molecule methods used in this work and Christine Jacobs-Wagner and for the generous use of their STORM microscope. We thank Magda Wąchalska for help in polysome profile. We thank Jennifer Ewald for stimulating discussions about cell growth and metabolism.

Reference

1. Karpinets, T. V., Greenwood, D. J., Sams, C. E. & Ammons, J. T. RNA: Protein ratio of the unicellular organism as a characteristic of phosphorous and nitrogen stoichiometry and of the cellular requirement of ribosomes for protein synthesis. *BMC Biol.* **4**, (2006).
2. Scott, M., Gunderson, C. W., Mateescu, E. M., Zhang, Z. & Hwa, T. Interdependence of Cell Growth and Gene Expression: Origins and Consequences. *Science* **330**, 1099–1102 (2010).
3. Paulo, J. A. *et al.* Quantitative mass spectrometry-based multiplexing compares the abundance of 5000 *S. cerevisiae* proteins across 10 carbon sources. *J. Proteomics* **148**, 85–93 (2016).
4. Metzl-Raz, E. *et al.* Principles of cellular resource allocation revealed by condition-dependent proteome profiling. *eLife* **6**, e28034 (2017).
5. Björkeroth, J. *et al.* Proteome reallocation from amino acid biosynthesis to ribosomes enables yeast to grow faster in rich media. *Proc. Natl. Acad. Sci.* **117**, 21804–21812 (2020).
6. Xia, J. *et al.* Proteome allocations change linearly with the specific growth rate of *Saccharomyces cerevisiae* under glucose limitation. *Nat. Commun.* **13**, (2022).
7. Elsemman, I. E. *et al.* Whole-cell modeling in yeast predicts compartment-specific proteome constraints that drive metabolic strategies. *Nat. Commun.* **13**, (2022).
8. Matamouros, S. *et al.* Growth-rate dependency of ribosome abundance and translation elongation rate in *Corynebacterium glutamicum* differs from that in *Escherichia coli*. *Nat. Commun.* **14**, 5611 (2023).
9. Dai, X. *et al.* Reduction of translating ribosomes enables *Escherichia coli* to maintain elongation rates during slow growth. *Nat. Microbiol.* **2**, 1–9 (2016).
10. Balakrishnan, R. *et al.* Principles of gene regulation quantitatively connect DNA to RNA and proteins in bacteria. *Science* **378**, eabk2066 (2022).
11. Lin, J. & Amir, A. Homeostasis of protein and mRNA concentrations in growing cells. *Nat. Commun.* **9**, 4496 (2018).
12. Chure, G. & Cremer, J. An optimal regulation of fluxes dictates microbial growth in and out of steady state. *eLife* **12**, e84878 (2023).

13. Sechkar, K., Steel, H., Perrino, G. & Stan, G. B. A coarse-grained bacterial cell model for resource-aware analysis and design of synthetic gene circuits. *Nat. Commun.* **15**, (2024).
14. Dai, X. & Zhu, M. Coupling of Ribosome Synthesis and Translational Capacity with Cell Growth. *Trends Biochem. Sci.* **45**, 681–692 (2020).
15. Waldron, C., Jundt, R. & Lacroute, F. Evidence for a High Proportion of Inactive Ribosomes in Slow-Growing Yeast Cells. *Biochem J* **168**, 409–415 (1977).
16. Bonven, B. & Gulløv, K. Peptide chain elongation rate and ribosomal activity in *Saccharomyces cerevisiae* as a function of the growth rate. *Mol. Gen. Genet. MGG* **170**, 225–230 (1979).
17. Guzikowski, A. R. *et al.* Differential translation elongation directs protein synthesis in response to acute glucose deprivation in yeast. *RNA Biol.* **19**, 636–649 (2022).
18. Lacroute, F. RNA and protein elongation rates in *Saccharomyces cerevisiae*. *Mol. Gen. Genet. MGG* **125**, 319–327 (1973).
19. Boehlke, K. W. & Friesen, J. D. Cellular content of ribonucleic acid and protein in *Saccharomyces cerevisiae* as a function of exponential growth rate: calculation of the apparent peptide chain elongation rate. *J. Bacteriol.* **121**, 429–433 (1975).
20. Waldron, C. & Lacroute, F. Effect of growth rate on the amounts of ribosomal and transfer ribonucleic acids in yeast. *J. Bacteriol.* **122**, 855–865 (1975).
21. Riba, A. *et al.* Protein synthesis rates and ribosome occupancies reveal determinants of translation elongation rates. *Proc. Natl. Acad. Sci. U. S. A.* **116**, 15023–15032 (2019).
22. Calabrese, L., Ciandrini, L. & Cosentino Lagomarsino, M. How total mRNA influences cell growth. *Proc. Natl. Acad. Sci.* **121**, e2400679121 (2024).
23. Sun, M. *et al.* Global Analysis of Eukaryotic mRNA Degradation Reveals Xrn1-Dependent Buffering of Transcript Levels. *Mol. Cell* **52**, 52–62 (2013).
24. García-Martínez, J. *et al.* The cellular growth rate controls overall mRNA turnover, and modulates either transcription or degradation rates of particular gene regulons. *Nucleic Acids Res.* **44**, 3643–3658 (2016).
25. Swaffer, M. P. *et al.* RNA polymerase II dynamics and mRNA stability feedback scale mRNA amounts with cell size. *Cell* **186**, 5254–5268.e26 (2023).
26. Heyer, E. E. & Moore, M. J. Redefining the Translational Status of 80S Monosomes. *Cell* **164**, 757–769 (2016).
27. Rahaman, S., Faravelli, S., Voegeli, S. & Becskei, A. Polysome propensity and tunable thresholds in coding sequence length enable differential mRNA stability. *Sci. Adv.* **9**, eadh9545 (2023).
28. Mäkelä, J. *et al.* Genome concentration limits cell growth and modulates proteome composition in *Escherichia coli*. *eLife* **13**, RP97465 (2024).
29. Kapadia, N. *et al.* Processive Activity of Replicative DNA Polymerases in the Replisome of Live Eukaryotic Cells. *Mol. Cell* **80**, 114–126.e8 (2020).
30. Ali, A. *et al.* Adaptive preservation of orphan ribosomal proteins in chaperone-dispersed condensates. *Nat. Cell Biol.* **25**, 1691–1703 (2023).
31. Zenklusen, D., Larson, D. R. & Singer, R. H. Single-RNA counting reveals alternative modes of gene expression in yeast. *Nat. Struct. Mol. Biol.* **15**, 1263–1271 (2008).
32. von der Haar, T. A quantitative estimation of the global translational activity in logarithmically growing yeast cells. *BMC Syst. Biol.* **2**, 87 (2008).

33. Paulo, J. A., O'Connell, J. D., Gaun, A. & Gygi, S. P. Proteome-wide quantitative multiplexed profiling of protein expression: Carbon-source dependency in *Saccharomyces cerevisiae*. *Mol. Biol. Cell* **26**, 4063–4074 (2015).
34. Melnikov, S. *et al.* One core, two shells: bacterial and eukaryotic ribosomes. *Nat. Struct. Mol. Biol.* **19**, 560–567 (2012).
35. Fukuda, T., Kawai-Noma, S., Pack, C.-G. & Taguchi, H. Large-scale analysis of diffusional dynamics of proteins in living yeast cells using fluorescence correlation spectroscopy. *Biochem. Biophys. Res. Commun.* **520**, 237–242 (2019).
36. Makhlof, L. *et al.* The UFM1 E3 ligase recognizes and releases 60S ribosomes from ER translocons. *Nature* **627**, 437–444 (2024).
37. Kraut-Cohen, J. *et al.* Translation- and SRP-independent mRNA targeting to the endoplasmic reticulum in the yeast *Saccharomyces cerevisiae*. *Mol. Biol. Cell* **24**, 3069–3084 (2013).
38. Jan, C. H., Williams, C. C. & Weissman, J. S. Principles of ER cotranslational translocation revealed by proximity-specific ribosome profiling. *Science* **346**, 1257521 (2014).
39. Martin-Perez, M. & Villén, J. Determinants and Regulation of Protein Turnover in Yeast. *Cell Syst.* **5**, 283–294.e5 (2017).
40. Christiano, R., Nagaraj, N., Fröhlich, F. & Walther, T. C. Global Proteome Turnover Analyses of the Yeasts *S. cerevisiae* and *S. pombe*. *Cell Rep.* **9**, 1959–1965 (2014).
41. Malina, C., Yu, R., Björkeroth, J., Kerkhoven, E. J. & Nielsen, J. Adaptations in metabolism and protein translation give rise to the Crabtree effect in yeast. *Proc. Natl. Acad. Sci.* **118**, e2112836118 (2021).
42. Ingolia, N. T., Ghaemmaghami, S., Newman, J. R. S. & Weissman, J. S. Genome-Wide Analysis in Vivo of Translation with Nucleotide Resolution Using Ribosome Profiling. *Science* **324**, 218–223 (2009).
43. Ingolia, N. T., Lareau, L. F. & Weissman, J. S. Ribosome Profiling of Mouse Embryonic Stem Cells Reveals the Complexity and Dynamics of Mammalian Proteomes. *Cell* **147**, 789–802 (2011).
44. Hou, W., Harjono, V., Harvey, A. T., Subramaniam, A. R. & Zid, B. M. Quantification of elongation stalls and impact on gene expression in yeast. *RNA* **29**, 1928–1938 (2023).
45. Torrent, M., Chalancon, G., De Groot, N. S., Wuster, A. & Madan Babu, M. Cells alter their tRNA abundance to selectively regulate protein synthesis during stress conditions. *Sci. Signal.* **11**, (2018).
46. Azizoğlu, A., Brent, R. & Rudolf, F. A precisely adjustable, variation-suppressed eukaryotic transcriptional controller to enable genetic discovery. *eLife* **10**, (2021).
47. Grosshans, H., Hurt, E. & Simos, G. An aminoacylation-dependent nuclear tRNA export pathway in yeast. *Genes Dev.* **14**, 830–840 (2000).
48. Dewe, J. M., Whipple, J. M., Chernyakov, I., Jaramillo, L. N. & Phizicky, E. M. The yeast rapid tRNA decay pathway competes with elongation factor 1A for substrate tRNAs and acts on tRNAs lacking one or more of several modifications. *RNA* **18**, 1886–1896 (2012).
49. Huang, H.-Y. & Hopper, A. K. In vivo biochemical analyses reveal distinct roles of β -importins and eEF1A in tRNA subcellular traffic. *Genes Dev.* **29**, 772–783 (2015).
50. Evans, M. E., Clark, W. C., Zheng, G. & Pan, T. Determination of tRNA aminoacylation levels by high-throughput sequencing. *Nucleic Acids Res.* **45**, e133–e133 (2017).

51. Srivastava, N. *et al.* A Dual Homeostatic Regulation of Dry Mass and Volume Defines a Target Density in Proliferating Mammalian Cells. 2025.04.24.650395 Preprint at <https://doi.org/10.1101/2025.04.24.650395> (2025).
52. Nguyen, V. Q. *et al.* Spatiotemporal coordination of transcription preinitiation complex assembly in live cells. *Mol. Cell* **81**, 3560–3575.e6 (2021).
53. Brito Querido, J., Díaz-López, I. & Ramakrishnan, V. The molecular basis of translation initiation and its regulation in eukaryotes. *Nat. Rev. Mol. Cell Biol.* **25**, 168–186 (2024).
54. Lanz, M. C. *et al.* Genome dilution by cell growth drives starvation-like proteome remodeling in mammalian and yeast cells. *Nat. Struct. Mol. Biol.* **31**, 1859–1871 (2024).
55. Lang, G. I. *et al.* Pervasive genetic hitchhiking and clonal interference in forty evolving yeast populations. *Nature* **500**, 571–574 (2013).
56. Venkataram, S. *et al.* Development of a Comprehensive Genotype-to-Fitness Map of Adaptation-Driving Mutations in Yeast. *Cell* **166**, 1585–1596.e22 (2016).
57. Laplante, M. & Sabatini, D. M. Regulation of mTORC1 and its impact on gene expression at a glance. *J. Cell Sci.* **126**, 1713–1719 (2013).
58. Albert, B. *et al.* Sfp1 regulates transcriptional networks driving cell growth and division through multiple promoter-binding modes. *Genes Dev.* **33**, 288–293 (2019).
59. Grimm, J. B. *et al.* A general method to improve fluorophores for live-cell and single-molecule microscopy. *Nat. Methods* **12**, 244–250 (2015).
60. Verschoor, A., Warner, J. R., Srivastava, S., Grassucci, R. A. & Frank, J. Three-dimensional structure of the yeast ribosome. *Nucleic Acids Res.* **26**, 655–661 (1998).
61. MGlinicy, N. J. & Ingolia, N. T. Transcriptome-wide measurement of translation by ribosome profiling. *Methods* **126**, 112–129 (2017).
62. Rouillon, A., Barbey, R., Patton, E. E., Tyers, M. & Thomas, D. Feedback-regulated degradation of the transcriptional activator Met4 is triggered by the SCF^{Met30} complex. *EMBO J.* **19**, 282–294 (2000).
63. Padovani, F., Mairhörmann, B., Falter-Braun, P., Lengefeld, J. & Schmoller, K. M. Segmentation, tracking and cell cycle analysis of live-cell imaging data with Cell-ACDC. *BMC Biol.* **20**, 174 (2022).
64. Phizicky, E. M. & Hopper, A. K. tRNA biology charges to the front. *Genes Dev.* **24**, 1832–1860 (2010).

Methods

Yeast strains and media conditions

All *S. cerevisiae* strains used in this study are in the *W303 MATa* background. The genotypes of all strains are listed in **Supplementary Table 1**. XG03, XG04, XG06 and XG07 were used to measure the active ribosome fraction by single molecule tracking (SMT). A sucrose cushion analysis confirmed that the Halo tag was successfully incorporated into the 80S ribosome. Strain XG48 (*P_{tet}-RPB1*) was used to assess changes in the active ribosome fraction under reduced mRNA levels. In this strain, the repressors TetR and TetR-Tup1 were integrated into the *URA3* locus, and an inducible promoter (*P_{7tet.1}*) was placed upstream of the *RPB1* gene⁴⁶. Similarly, strain XG61 (*P_{tet}-TEF1, tef2Δ*) was used to change eEF1A expression. MS165 was used to measure the DNA-bound Rpb1 fraction by SMT²⁵. Strain ML127 was used for the G1 arrest experiments⁵⁴. ZY478 and ZY483 were used to measure the onset of luminescence from Nluc reporters with variable-length upstream coding sequences under different carbon sources^{21,40}.

For carbon-limited conditions, yeast cells were cultured in medium prepared with low-fluorescence yeast nitrogen base (LF-YNB, Formedium CYN6205) to reduce background fluorescence in single-molecule experiments, along with a complete amino acid dropout mix. One of the following 12 carbon sources (2% w/v) was added as the sole carbon source: fructose, glucose, sucrose, mannose, acetate, galactose, lactate, ethanol, pyruvate, glycerol, trehalose, or melibiose. For nitrogen-limited conditions, yeast cells were cultured in a medium prepared with LF-YNB and supplemented only with the minimal required auxotrophic supplements: tryptophan, uracil, and histidine. One of the following carbon and nitrogen source combinations were added: 2% glucose + 20 mM glutamic acid, 2% galactose + 20 mM glutamic acid, or 2% glucose + 20 mM leucine.

The pH of all media was adjusted to 6.0 using NaOH. For G1 arrest experiments, cells were grown in SC + 2% glycerol+ 1% ethanol. For the XG48 (*P_{tet}-RPB1*) strain, cells were grown in SC + 2% glucose and 5-200 ng/ml aTc. Unless stated otherwise, cells were grown at 30 °C for at least 10 doublings before the experiment was conducted. Cells were harvested at an OD600 between 0.1 and 0.4 for subsequent measurements.

Growth rate measurements

To measure the growth rate of cells in a specific growth condition, cells were cultured to the exponential phase and then diluted into a pre-heated flask with 50 ml of fresh media

(OD600=0.01). Cells were incubated at 30 °C and OD600 was measured every 1-2 hours. To determine the specific growth rate, log-transform OD600 values were plotted against time, and the slope of this log(OD600) versus time plot was calculated as the specific growth rate. The population doubling time can then be calculated as $\ln 2/\text{growth rate}$. There were at least two replicates of the growth rate measurement for each condition.

LC-MS/MS sample preparation and data acquisition

A 10 mL yeast culture (OD600=0.2) was harvested, snap-frozen, and stored at -80 °C. 1mM PMSF and protease inhibitors (1 tablet/10 mL) were then added to the lysis buffer (50 mM Tris-HCl pH 8.0, 0.2% Tergitol, 150 mM NaCl, 5 mM EDTA). Cells were then resuspended from in the lysis buffer, and lysed using a FastPrep-24 (4 °C, 5.5 m/s, 35 s). The lysate was then centrifuged (15,000 × g, 5 min, 4 °C) and the supernatant collected. SDS was then added to 1%, DTT to 5 mM, and the sample was incubated at 65 °C for 15 min. Then, 15 mM Iodoacetamide was added before incubation at room temperature for 15 min. Proteins were then precipitated by adding >3 volumes PPT solution (acetone:ethanol:acetic acid = 50%:49.9%:0.1%) followed by incubation on ice for 15 min and centrifugation (17,000 × g, 5 min, 4 °C). The supernatant was discarded and the pellet washed with 500 µL PPT solution. The sample was then centrifuged again, the supernatant discarded, and the pellet was air dried for ~10 min. The pellet was then resuspended in fresh 75 µL urea/Tris solution (8M urea, 50 mM Tris-HCl pH=8.0) before adding 225 µL 150 mM NaCl solution. The sample was digested overnight at 37 °C with trypsin (1:50 enzyme:protein), with agitation. The next day, 15 µL 10% TFA (Trifluoroacetic acid) was added to stop digestion and the sample was centrifuged (17,000 × g, 2 min), and the supernatant recovered. The supernatant was then desalted using a C18 Cartridge (Waters #WAT054955). Aliquots were then stored at -20 °C.

Desalted peptides were analyzed on a Fusion Lumos mass spectrometer (Thermo Fisher Scientific) equipped with a Thermo EASY-nLC 1200 LC system (Thermo Fisher Scientific). Peptides were separated by capillary reverse-phase chromatography on a 25-cm column (75-µm inner diameter, packed with 1.6-µm C18 resin, cat. no. AUR2-25075C18A, Ionopticks). Peptides were introduced into the Fusion Lumos mass spectrometer using a 125-min stepped linear gradient at a flow rate of 300 nL min⁻¹. The steps of the gradient are as follows: 3–27% buffer B (0.1% (v:v) formic acid in 80% acetonitrile) for 105 min, 27–40% buffer B for 15 min, 40–95% buffer B for 5 min and finally maintaining at 90% buffer B for 5 min. Column temperature was maintained at 50 °C throughout the procedure. Xcalibur software (v.4.4.16.14, Thermo Fisher Scientific) was used for the data acquisition and the instrument was operated in data-

dependent mode. Advanced peak detection was enabled. Survey scans were acquired in the Orbitrap mass analyzer (Profile mode) over the range 375–1,500 m/z with a mass resolution of 240,000 (at m/z 200). For MS1, the normalized AGC target (%) was set at 250 and maximum injection time was set to 'Auto'. Selected ions were fragmented by higher-energy collisional dissociation with normalized collision energies set to 31 and the fragmentation mass spectra were acquired in the ion trap mass analyzer with the scan rate set to 'Turbo'. The isolation window was set to the 0.7-m/z window. For MS2, the normalized AGC target (%) was set to 'Standard' and maximum injection time to 'Auto'. Repeated sequencing of peptides was kept to a minimum by dynamic exclusion of the sequenced peptides for 30 s. Maximum duty cycle length was set to 1 s.

All raw files were searched using the Andromeda engine embedded in MaxQuant (v.2.4.2). Variable modifications included oxidation (M) and protein amino-terminal acetylation. Carbamidomethyl (C) was a fixed modification. The number of modifications per peptide was capped at five. Digestion was set to tryptic (proline blocked). MaxLFQ was used to determine the summed ion intensity for each protein. The database search was conducted using the UniProt proteome—Yeast_UP000002311_559292. The minimum peptide length was seven amino acids. The 1% false recovery rate (FDR) was determined using a reverse decoy proteome.

Immunoblotting

Ten µl cultures were grown to an OD600 of 0.1, harvested, snap-frozen, and stored at –80 °C. Cell pellets were resuspended in urea lysis buffer and lysed using a FastPrep-24 instrument (5.5 m/s for 40 s at 4 °C). Lysates were clarified by centrifugation at 17,000 × g for 10 min at 4 °C, and the supernatant was recovered. Protein concentrations were determined using the Protein Assay Dye (Bio-Rad). Then, equal amounts of protein were loaded on 10% Tris-glycine SDS-PAGE gels and transferred to nitrocellulose membranes using the iBlot 2 Dry Blotting System (Invitrogen). The following primary antibodies were used for Immunoblotting at 1:1000 dilution: Anti-HaloTag (rabbit, Polyclonal, Promega #G928A), Anti-Rpb1 (mouse, monoclonal, Sigma-Aldrich #05-952-I), Anti-eEF1A (mouse, monoclonal, Sigma-Aldrich #05235), and Anti-Actin (rabbit, polyclonal, Sigma-Aldrich #A2103). Primary antibodies were detected using the following fluorescently labeled secondary antibodies at 1/10,000 dilution: Alexa Fluor 680 Goat anti-Mouse (Invitrogen #A21058), IRDye 680RD Goat anti-Rabbit (LI-COR # 926-68071), Alexa Fluor 790 Goat anti-Rabbit (Invitrogen #A11369), and IRDye 800CW Goat anti-Mouse (LI-COR # 926-32210). Membranes were imaged on a Typhoon biomolecular imager.

Single-molecule tracking to determine the active ribosome fraction and the DNA-bound RNAP II fraction

To prepare samples for tracking single ribosome molecules, cells are cultured for more than 10 doublings before harvesting (OD₆₀₀=0.1-0.3). JF-PA549 Halotag (Janelia Farms photoactivatable 549) dye was added at a final concentration of 1 nM for ribosomal protein-Halo fusion strains and 10 nM for *RPB1-Halo* strain⁵⁹. Cultures were incubated at 30 °C for 40 min and then pelleted. Cells then washed three times in fresh media to remove unbound dye and resuspend in 15 µl media. A 65 µl gene frame (1.5*1.6 cm) was glued to the slide and the SC culture solution containing the specific carbon source was added. 4 µl of cell culture was placed on the surface of an agarose slide containing the nutrient condition of interest and spread evenly by a pipette tip or clean stick.

Live cell photoactivated localization microscopy (PALM) was performed on a Nikon N-STORM microscope equipped with a Perfect Focus System and a motorized stage. JF549 was detected using an iXon3 DU 897 EMCCD camera (Andor) and excited using a 50 mW 561 nm laser (MLC400B laser unit, Agilent) at 30 °C. The laser was focused through a 100x Apo TIRF 1.49 NA oil immersion objective (Nikon) onto the sample using an angle for highly inclined thin illumination to reduce background fluorescence. Fluorescence emission was filtered by a C-N Storm 405/488/561/647 laser quad set. Transmission illumination was used to gather brightfield images.

PALM experiments were performed by using continuous activation of molecules with low power (0.1% – 5% in NIS-element software) 405 nm light to photo activate around 1-2 molecules/cell at the same time. Simultaneous fast-exposure (15 ms) illumination with 561 nm light (50% in NIS-element software) was then used to image molecules. PALM movies of 10,000 frames were acquired with continuous laser illumination and a camera frame rate of 37 ms. A bright field picture was taken to determine the cell area.

After imaging, single particle tracking was performed by Trackmate on ImageJ software. Molecules were localized in each frame using a Laplacian of Gaussian (LoG) method with an estimated diameter of 1 µm. A trajectory allows a maximum of 2 µm of movement within a frame, and a single frame disappearance within a trajectory was allowed. The diffusion coefficient of a single molecule (D_a) can be calculated from the stepwise mean-squared displacement (MSD) of its trajectory:

$$D_a = \frac{1}{4n\Delta t} \sum_{i=1}^n [x(i\Delta t) - x(i\Delta t + \Delta t)]^2 + [y(i\Delta t) - y(i\Delta t + \Delta t)]^2$$

where $x(t)$ and $y(t)$ denote the coordinates of the ribosome of interest at time t . Δt is the time between two consecutive frames, and n is the total steps in the trajectory. The ribosome trajectories with less than 9 displacements were omitted.

Polysome profile measurements

Yeast cells were grown in 100 mL SC medium with different carbon sources at 30°C until the culture reached an OD600 of approximately 0.5. To stabilize ribosomes, cycloheximide (CHX) was added at a final concentration of 100 µg/mL for 5 min before harvesting. Cells were collected by centrifugation at 3,000×g for 5 min at 4°C, and the pellet was then stored at -80°C. The cell pellet was resuspended in a pre-chilled lysis buffer A (20 mM Tris-HCL, pH 7.4; 50 mM KCl; 10 mM MgCl₂; 1 mM DTT added immediately prior to use). Cells were lysed using a Fastprep 24 (settings: 5.5 m/s, 1 x 35 seconds) at 4 °C, followed by 5 min on ice. This process was repeated 6 times. The lysate was then clarified by centrifugation at 3,000×g for 5 min at 4°C, then by centrifugation at 11300×g, at 4°C for 2 and 10 min, respectively. The supernatant, which contains ribosomes, was then collected for gradient separation.

A 4.5–45% (w/v) sucrose gradient was prepared in buffer A in a 13.2 mL tube using a Biocomp Gradient Master. The sucrose gradient was stored at 4°C for at least 1 hour. Equivalent numbers of OD260 units (10 units) in a total volume of 200 ml Buffer A was then loaded on the 4.5–45% sucrose gradients. 200 ml Buffer A without cell lysis was also loaded on a sucrose gradient as a blank. Then, the samples were centrifuged at 35,000 rpm for 2 hours and 10 min at 4°C on a SW41 Ti rotor in a Beckman ultracentrifuge. After centrifugation, the gradient is fractionated from the top, and absorbance at 254 nm is continuously monitored to reveal the polysome profile by a Biocomp Piston Gradient Fractionator.

To estimate the active ribosome fraction by polysome profile data, we first subtracted the signal of a blank sample from the signal absorbance at 254 nm. For 40S and 60S ribosome subunits, the signal was integrated from the region indicated on **Extended Data Fig. 2c**. Because each ribosome contains roughly 5500 bp of rRNA and the average mRNA length is about 1250 bp, the rRNA fraction in the monosome is approximately 82%⁴. Thus, we multiplied the integrated monosome signal by 0.82 to obtain its rRNA contribution. For polysomes containing two ribosomes, a factor of 0.90 was used. Similarly, larger polysomes were corrected using their respective rRNA fractions. All polysomes were assumed to be active, and all other ribosomes were considered inactive to calculate the active ribosome fraction. Accordingly, the active ribosome fraction was calculated as polysome signal over total signal: $(\text{polysome})/(\text{40s}+\text{60s}+\text{monosome}+\text{polysome})$.

Estimate average peptide elongation rate of active ribosomes

We estimate the average peptide elongation rate of a single ribosome by the synthesis rate of the total protein. Since yeast grows exponentially, the protein mass increases at

a rate proportional to the existing protein mass, m_{prot} , so that $\frac{dm}{dt} = \lambda m = \frac{m \ln 2}{T_d}$, where lambda is the growth rate and T_d is the population doubling time. the rate of protein mass increase is given by the number of translating ribosomes, N_{ribo} , and the average peptide elongation rate for all ribosomes, e_r , so that:

$$e_r = \frac{m_{prot} \ln 2}{N_{ribo} T_d}.$$

We now consider the fact that only some ribosomes are active. If the active ribosome fraction is ϕ_a , and the average elongation rate of an active ribosome c_p is:

$$c_p = \frac{m_{prot} \ln 2}{\phi_a N_{ribo} T_d}.$$

We define the ribosome fraction in the proteome as ϕ_r , and the average protein mass of a single ribosome as m_{rb} so that the average ribosomal protein mass in the cell population is:

$$m_{prot} \phi_r = N_{ribo} m_{rb}.$$

Then, the average elongation rate of an active ribosome can be rewritten as

$$c_p = \frac{m_{rb} \ln 2}{\phi_a \phi_r T_d}.$$

The average protein mass of a single ribosome m_{rb} is ~11984 amino acids ^{12,60}. The remaining three parameters (ribosome fraction in the proteome ϕ_r , active ribosome fraction ϕ_a and doubling time T_d) were obtained from the measurements in this study.

Since $\frac{\ln 2}{\lambda} = T_d$, the growth rate λ can be calculated as:

$$\lambda = \frac{c_p \phi_a \phi_r}{m_{rb}} .$$

Ribosome footprinting

Yeast cells were cultured in 200 mL synthetic complete (SC) medium containing various carbon sources at 30 °C until the cultures reached an OD600 of ~0.5 for ribosome footprinting⁶¹. Cells were harvested by vacuum filtration (GenClone), scraped from the filter membrane with a spatula, immediately snap-frozen in liquid nitrogen, and stored at –80 °C. Cell pellets were resuspended in 300 µL of ice-cold lysis buffer (20 mM Tris-HCl, pH 7.4; 150 mM NaCl; 5 mM MgCl₂; 1 mM DTT; 1% [v/v] Triton X-100; 25 U/mL Turbo DNase I; 100 µg/ml cycloheximide) and lysed using a FastPrep-24 instrument (5.5 m/s for 35 s) at 4 °C. After each 35 s cycle, samples were incubated on ice for 5 min; this cycle was repeated six times. Lysates were clarified by centrifugation at 3,000 × g for 5 min at 4 °C, and the supernatant was transferred to a fresh tube and centrifuged again at 20,000 × g for 10 min at 4 °C. Then, 800 µg of total RNA was diluted to 200 µL with lysis buffer and treated with 1.5 µL RNase I for 45 min at room temperature. Digestion was terminated by adding 10 µL RNase Inhibitor (SUPERase-In, Invitrogen). A 4.5–45% (w/v) sucrose gradient was prepared in polysome buffer (20 mM Tris-HCl, pH 7.4; 150 mM NaCl; 5 mM MgCl₂; 1 mM DTT) in a 13.2 mL ultracentrifuge tube using a Biocomp Gradient Master and equilibrated at 4 °C for at least 1 h.

Two hundred µL of the RNase-treated lysate was gently layered onto each gradient and centrifuged at 36,000 rpm for 2 h at 4 °C on a SW41 Ti rotor in a Beckman Optima XE90 ultracentrifuge. Gradients were then fractionated from the top while continuously monitoring A254 with a Biocomp Piston Gradient Fractionator. Then, the fraction containing monosomes was collected. Monosome fractions were adjusted to 1% (w/v) SDS and 200 µg/mL proteinase K (Thermo), mixed by gentle inversion, and incubated at 42 °C for 30 min. Phenol:chloroform:isoamyl alcohol (25:24:1) was added to the proteinase K-treated fractions in a 1:1 ratio, vortexed vigorously, and centrifuged at 16,000 × g for 5 min at room temperature. The upper aqueous phase was transferred to a fresh tube, and RNA was precipitated by adding 0.1 volume of 3 M sodium acetate (pH 5.2), 2.5 volumes of 100% ethanol, and 1 µL glycogen, followed by incubation at –20 °C overnight. Precipitated RNA was pelleted by centrifugation at 20,000 × g for 30 min at 4 °C. The supernatant was then carefully removed, and the pellet was air-dried on ice for 10 min. Finally, RNA was resuspended in 5 µL of 10 mM Tris (pH 8.0). Samples were mixed 1:1 with RNA loading dye (NEB B0363S), denatured at 80 °C for 90 s, and resolved on a 15% polyacrylamide TBE-urea gel at 200 V for 60 min. Gels were stained with 1× SYBR Gold in TBE running buffer, visualized under UV

illumination, and the 17–34 nt region was excised into a fresh tube. Excised gel slices were incubated in 400 µL RNA extraction buffer (300 mM sodium acetate, pH 5.5; 1 mM EDTA; 0.25% [v/v] SDS) overnight at room temperature to elute the RNA. The eluate was precipitated with ethanol (or isopropanol) as described above, and then pelleted by centrifugation, air-dried on ice, and resuspended in 4 µL of 10 mM Tris-HCl (pH 8.0). Recovered RNA (3.5 µL) was treated with T4 polynucleotide kinase by adding 0.5 µL 10× T4 PNK buffer, 0.5 µL T4 PNK (NEB), and 0.5 µL SUPERase•In, then incubating at 37 °C for 30 min to repair 2'–3' cyclic phosphates. NEBNext Small RNA Library Prep Set (E7330S) was used to build libraries for pair-end (2×150 bp) Illumina sequencing (GENEWIZ). 15 million reads were recorded per sample.

Raw paired-end reads were first processed with Trimmomatic v0.39 to remove adapter sequences and perform quality trimming. We retained only reads ≥ 15 nt. Low-quality bases were trimmed using default parameters. Trimmed reads were then aligned against the *S. cerevisiae* rRNA reference sequence (SGD S288C; http://sgd-archive.yeastgenome.org/sequence/S288C_reference/rna/) using Bowtie v1.2.3 with options -f -v 2 -k 1 -p 4. Reads mapping to rRNA were discarded. The remaining non-rRNA reads were mapped to the *S. cerevisiae* genome (NCBI R64) with Bowtie (-m 1) to retain only uniquely aligned fragments. Finally, these uniquely mapped reads were aligned to the *S. cerevisiae* transcriptome (NCBI R64) to produce BAM files for subsequent analysis of ribosome footprints to calculate translation efficiency.

Calculation of translation efficiency

Here, we calculate the translation efficiency of each gene based on spike-in RNA-seq and ribo-seq across four growth conditions⁴³. The normalized ribosome footprint density for each gene was obtained by dividing the number of ribosome footprint reads mapped to its coding sequence (CDS) by the CDS length, and then normalizing this value to the total number of ribosome footprint reads mapped to the yeast transcriptome. Similarly, the normalized mRNA read density was calculated by dividing the number of mRNA reads mapped to the CDS by the CDS length, followed by normalization to the total mRNA reads. Genes with fewer than 20 reads were excluded from the analysis. The translation efficiency (TE) of each gene in each condition can then be calculated as:

$$TE = \frac{\text{norm. RFs density}}{\text{norm. mRNA density}} .$$

Measure the translation onset time using a luciferase reporter

Two constructs were analyzed: *P_{tet}-Nluc* (ZY478) and *P_{tet}-YFP-Nluc* (ZY483), the latter containing a 315-amino-acid YFP insert upstream of Nluc¹⁷. Cells were grown in SC medium containing either glucose or glycerol at 30 °C to an OD600 of 0.1. For each strain and condition, 150 µL of culture was dispensed into wells of a black 96 well plate (Cellvis). One set of wells was supplemented with 250 ng/mL anhydrotetracycline (aTc) and 5 µM furimazine, while control wells received only 5 µM furimazine. Plates were incubated in a microplate reader (BioTek) at 30 °C, and bioluminescence along with OD600 was measured every 30 s for 60 min, with a 3 s orbital shake prior to each reading. Three biological replicates were performed for each condition.

Raw bioluminescence values were first normalized to cell density by dividing each reading by the corresponding OD600. Next, luminescence in the presence of aTc was background-corrected by subtracting the signal from the uninduced control. These background-corrected values were then baseline-corrected using the mean of the first five time points. Relative light units (RLU) were then square-root transformed. Translation onset time was estimated by performing linear regression on the square-root transformed data in its linear region (Schleif plot). The x-intercept of this fit approximates the time required to translate the upstream coding sequence.

RT-qPCR to determine the tRNA abundance

We measured tRNA abundance by RT-qPCR in yeast cells cultured with five different carbon sources (glucose, mannose, galactose, glycerol, and trehalose). Cultures were grown to an OD600 of 0.1, and 20 mL of each culture was harvested, snap-frozen, then stored at –80 °C. Cells were lysed at 4 °C using a FastPrep 24 instrument (5.5 m/s, 40 s), and total RNA was extracted with the Direct-zol RNA Microprep Kit (Zymo Research). All RNA samples had A260/A230 and A260/A280 ratios above 2.

For cDNA synthesis, 1 µg of RNA was reverse-transcribed using SuperScript VILO Master Mix (Thermo Fisher), with the reaction carried out at 60 °C for 30 min to mitigate potential effects of tRNA secondary structures and modifications. The resulting cDNA was stored at –20 °C until further use. One µL of cDNA was diluted 1:100 for qPCR, which was performed using iTaq Universal SYBR Green Supermix (Bio-Rad #1725121). The 42 tRNA primer pairs we used were taken from Torrent et al⁴⁵. Two biological replicates were performed per experiment and 2 technical replicates were performed per biological replicate.

To normalize tRNA levels, we selected three housekeeping genes (*PLN1*, *RNR2*, and *PRC1*), whose mRNA concentrations remained consistent across the different carbon sources, as indicated by our spike-in mRNA sequencing data (**Extended Fig. 4a**). The geometric mean of these housekeeping genes served as the reference for calculating

tRNA concentrations, and relative expression levels were determined using the standard $\Delta\Delta C_t$ method.

Spike-in RNA-seq to determine total mRNA concentration

Global mRNA concentration in different growth conditions was quantified by spike-in RNA sequencing. Ten milliliters of *S. cerevisiae* cultures (OD600=0.1-0.2) in different growth conditions were harvested by centrifugation at 12,000 × g for 30 s, snap-frozen in liquid nitrogen, and stored at −80 °C. As an external spike-in control, 5 mL *C. glabrata* was grown in SC medium with 2% glucose to an OD600 of ~0.2, then harvested, snap-frozen, and stored at −80 °C.

For spike-in normalization, the *C. glabrata* pellet was resuspended in 50 µL ice-cold PBS and combined with the *S. cerevisiae* pellet by gentle mixing. Twenty microliters of the mixed cells were removed and stored at −20 °C for genomic DNA sequencing. The remaining 30 µL was lysed in 300 µL TRI Reagent (Zymo Research) for total RNA extraction, following the manufacturer's protocol.

For total RNA sequencing, 30 µL of mixed cells were lysed in a FastPrep-24 instrument (5.5 m/s for 35 s at 4 °C). Lysates were clarified by centrifugation at 20,000 × g for 5 min at 4 °C, and the supernatant was retained. Total RNA was purified using the Direct-zol RNA Microprep Kit (Zymo Research) following the manufacturer's instructions. Purified RNA was submitted to GENEWIZ for mRNA library preparation and sequenced on an Illumina HiSeq (2×150 bp), yielding >20 million paired-end reads per sample. Raw reads were trimmed with fastp v0.23.1 to remove adapter sequences and low-quality bases. A combined *S. cerevisiae* (sacCer3, R64) and *C. glabrata* (CGD assemblies) reference genome was built, and trimmed reads were aligned to this reference using STAR v2.5.2b. Then, in mixed *S. cerevisiae* and *C. glabrata* sequencing libraries, transcript-per-million (TPM) values for each gene were calculated by standard method.

Genomic DNA was extracted using the YeaStar Genomic DNA Kit (Zymo Research) according to the manufacturer's chloroform protocol. Purified gDNA libraries were prepared and sequenced by GENEWIZ on an Illumina HiSeq platform (2×150 bp), generating >3 million paired-end reads per sample. Paired-end RNA-seq reads were trimmed to remove adapters and low-quality bases using *Trimmomatic* (v0.39). Clean reads were quantified with *Salmon* (v1.10) against a combined transcriptome reference of *Saccharomyces cerevisiae* (sacCer3, R64) and *Candida glabrata* (CGD assemblies). Transcript abundances were reported as Transcripts Per Million (TPM).

Then, the relative mRNA amount per genome of yeast in a given growth condition is then calculated as:

$$\text{mRNA amount per genome} = \left(\frac{\sum \text{TPM}_{S. cerevisiae}}{\sum \text{TPM}_{C. glabrata}} \right) \bigg/ \left(\frac{\sum \text{gDNA reads}_{S. cerevisiae}}{\sum \text{gDNA reads}_{C. glabrata}} \right),$$

which is used for calculating total mRNA concentration (see **Methods**).

Cell size measurements

Cells were cultured in different growth conditions at 30 °C to an OD600 of 0.1–0.2. Cultures were briefly sonicated to disperse cell clumps and then diluted 1:100 in Isoton II diluent (Beckman Coulter, #8546719). Cell volumes were measured on a Beckman Coulter Z2 counter following the manufacturer's protocol. Measurements <10 fL or >300 fL were excluded from downstream analysis.

DNA content analysis

Four hundred µL of yeast culture in different growth conditions were fixed by adding 1 mL ice-cold 100% ethanol and incubating at 4 °C for 30 min. Fixed cells were pelleted (3,000 × g, 5 min, 4 °C) and washed twice with PBS. Pellets were resuspended in 50 mM sodium citrate (pH 7.2), treated with RNase A (0.2 mg/mL) at 37 °C overnight, then with proteinase K (0.4 mg/mL) at 50 °C for 1–2 h. Samples were stained with 16 µg/mL propidium iodide (Invitrogen) for 30 min at room temperature in the dark, sonicated briefly to disperse clumps, and analyzed on an Attune NxT flow cytometer (YL1-A channel), collecting >30,000 events per sample. Single-cell events were gated in FlowJo to exclude debris and aggregates, and the mean YL1-A fluorescence intensity was taken as the genomes per cell.

Calculation of total mRNA concentration

To calculate the total mRNA concentration, we measured the relative mRNA amount per genome by spike-in RNA sequencing, the mean cell volume by Coulter counter, and genomes per cell by flow cytometry (see **Methods** described above). Relative mRNA amount per cell was then calculated as:

$$\text{mRNA amount per cell} = (\text{mRNA amount per genome}) \times (\text{genomes per cell}).$$

Then, total mRNA concentration was obtained by dividing mRNA amount per cell by the mean cell volume:

$$\text{total mRNA concentration} = \frac{\text{mRNA amount per cell}}{\text{mean cell volume}}.$$

Extended Data Fig. 5b shows a schematic of this workflow for quantifying total mRNA concentration.

Flow cytometry measurements of global protein concentration

Yeast cultures were grown to an OD₆₀₀ of 0.1, and 500 µL of culture was mixed with 500 µL of ice-cold 70% ethanol and incubated at 4 °C for 30 min to fix the cells. Fixed cells were washed twice with PBS and then resuspended in PBS containing 1 µg/mL Alexa Fluor 647 NHS Ester. Cells were stained for 1 h at room temperature in the dark, followed by three washes in PBS and brief sonication to disperse aggregates. Stained cells (>50,000 events per sample) were analyzed on an Attune NxT flow cytometer. Total protein fluorescence was recorded in the BL1-A channel, and forward scatter area (FSC-A) was used as an estimate of cell size. A robust linear regression of BL1-A versus FSC-A was performed for each sample, and the slope of the fitted line was taken as the measure of total protein concentration per unit cell volume.

RT-qPCR to determine the mRNA decay rate

Yeast cells were grown in methionine-free SC medium with one of four carbon sources (glucose, galactose, glycerol, or trehalose) at 30 °C to mid-log phase. To shut off MET3/MET17 transcription, methionine was added to a final concentration of 1 mM⁶². At 0, 6, 10, 14, 18, and 22 min after addition, 1 mL culture aliquots were harvested by centrifugation (17,000 × g, 30 s), immediately snap-frozen in liquid nitrogen, and stored at –80 °C.

Cell pellets were lysed in 300 µL TRI Reagent (Zymo Research) using the FastPrep-24 (5.5 m/s for 30 s at 4 °C). Lysates were clarified (13,000 rpm, 2 min, 4 °C) and total RNA purified with the Direct-zol RNA Microprep Kit (Zymo Research, #R2061). One microgram of RNA was reverse-transcribed with SuperScript VILO Master Mix (Thermo Fisher), and cDNA was diluted 1:100 for quantitative PCR. RT-qPCR was performed using iTaq Universal SYBR Green Supermix (Bio-Rad, #1725121) with *ACT1* as the internal control.

For each time course, two biological replicates were assayed, each with two technical replicates. Standard ΔC_t values were plotted against time, and the slope of the linear regression was taken as the mRNA decay rate.

Nuclear-to-cell volume fraction measurements

Yeast cells expressing Pus1-eGFP were grown in SC medium with different nutrients at 30 °C to log phase (OD600=0.1-0.2). Cells were harvested by brief centrifugation (2,500 rpm, 3 min), and the pellet was gently resuspended and mounted on an agarose slide (see single molecule tracking section for a detailed description of the agarose slide).

Imaging was performed on a Zeiss Axio Observer.Z1 wide-field epifluorescence microscope equipped with a 63×/1.4 NA oil-immersion objective and a Colibri LED module. eGFP fluorescence (Pus1-eGFP) was excited using the 505 nm LED at 25% intensity with a 1 s exposure. Phase-contrast images were captured to delineate cell outlines. A TempController 37-2 unit maintained the sample at 30 °C throughout acquisition. For each condition, z-stacks were collected, and the plane with maximum focus was selected by eye. Over 500 cells were imaged per replicate.

Cell boundaries were segmented automatically using ACDC software⁶³ and manually calibrated, and nuclear regions were defined via a custom Python algorithm from fluorescence images. To calculate cell volume V_{cell} , each yeast cell was approximated as a prolate spheroid. Cross-sections perpendicular to the long axis were summed, and for budding cells the mother and bud volumes were computed separately and then combined. The nucleus was modeled as a tri-axial ellipsoid: the long (a) and short (b) axes were measured in 2D using the skimage package, the third axis (c) was set to $c = \frac{a+b}{2}$, and volume was calculated as $V_{nucleus} = \frac{4}{3}\pi abc$. For each cell, the nuclear-to-cell volume fraction was calculated as nuclear volume divided by cell volume.

mRNA transcription model

Our model for mRNA dynamics is based on mass action kinetics of free nuclear RNAP II and the genome coupled with first order decay of mRNA at a rate that was found to be independent of the growth conditions (**Fig. 3e**). The DNA-bound RNAP II concentration, $[pol_{bound}]$, in the nucleus is determined by mass action with the genome, $[DNA]$, and the free nuclear RNAP II, $[pol_{free}]$, so that:

$$\frac{d[pol_{bound}]}{dt} = k_{on}^{pol}[DNA][pol_{free}] - k_{off}^{pol}[pol_{bound}],$$

where k_{on}^{pol} and k_{off}^{pol} are the binding and unbinding rates, respectively. At steady-state, we see that

$$k_{on}^{pol}[DNA][pol_{free}] - k_{off}^{pol}[pol_{bound}] = 0.$$

We consider the fraction of RNAP II in the proteome, ϕ_{pol} , to be equal to the sum of all subunits, so the concentration of RNAPII in nucleus is given as

$$[pol_{free}] + [pol_{bound}] = [pol_{total}] = P\phi_{pol} \frac{V_{cell}}{V_{nucleus}},$$

where P is the global protein concentration, V_{cell} is the cell volume, and $V_{nucleus}$ is the nuclear volume. We denote the ratio of nuclear-to-cell volume as $f = V_{nucleus}/V_{cell}$.

Substituting this into the above equation, the nuclear DNA-bound RNAP II concentration at steady-state can be written as:

$$[pol_{bound}] = \frac{P\phi_{pol}}{f \left(1 + \frac{k_{off}^{pol}}{k_{on}^{pol}[DNA]} \right)}.$$

Since the DNA concentration in the nucleus equals the DNA amount divided by the

nuclear volume, $[DNA] = \frac{DNA}{V_{nucleus}}$, we can rewrite the above equation as:

$$[pol_{bound}] = \frac{P\phi_{pol}}{f \left(1 + \frac{K_d^{pol} V_{cell} f}{DNA} \right)},$$

where $K_d^{pol} = k_{off}^{pol}/k_{on}^{pol}$ is the dissociation constant of RNAPII and the genome. The fraction of DNA-bound RNAPII is:

$$\frac{[pol_{bound}]}{[pol_{total}]} = \frac{1}{1 + \frac{K_d^{pol} V_{cell} f}{DNA}}.$$

For each growth condition, we can determine the cell volume with a Coulter counter (**Extended Data Fig. 5d**), and the nuclear-to-cell volume ratio with the Pus1-eGFP nuclear marker and a fluorescence microscope (**Fig. 3f**). Assuming the average DNA content in G1 phase is normalized to 1, the DNA content in different growth conditions can be determined by flow cytometry (**Extended Data Fig. 5c**). Thus, we can fit the model results with the single-molecule tracking data using only one free parameter K_d^{pol} . Fitting was performed using nonlinear least-squares regression using MATLAB's fitnlm function.

From the level of DNA-bound RNAPII and the constant mRNA decay rate, we can estimate the cellular mRNA concentration. mRNA is produced by RNAP II transcription

in the nucleus at a rate $k_{trans}^{mRNA} [pol_{bound}]$, quickly exported to cytoplasm, and then degraded at a rate k_d^{mRNA} . Assuming that the timescale of mRNA production and degradation is much faster than that of cell growth, the system can be treated as being in steady state so that:

$$\frac{d[mRNA]}{dt} = k_{trans}^{mRNA} [pol_{bound}] f - k_d^{mRNA} [mRNA] = 0,$$

which can be solved for the mRNA concentration to yield:

$$[mRNA] = \frac{k_{trans}^{mRNA} P \phi_{pol}}{k_d^{mRNA} \left(1 + \frac{K_d^{pol} V_{cell} f}{DNA} \right)}.$$

Here, global protein concentration (**Extended Data Fig. 5f**), RNAP II fraction in proteome (**Fig. 3c**) and mRNA decay rate (**Fig. 3d**) were all measured. Based on the fitted dissociation constant K_d^{pol} , we estimated the mRNA production rate k_{trans}^{mRNA} by fitting the model using our measurements of the total mRNA concentration (**Fig. 3a**). Fitting was performed using the nonlinear least-squares regression in MATLAB's fitnlm function.

mRNA-ribosome translation model

Given the ribosome and mRNA concentrations as inputs, we construct a mass action kinetic model for protein translation that predicts the active ribosome fraction and cell growth rate. For simplicity, we ignore the assembly process of the 40S and 60S subunits and simply view the ribosome as being a single molecular complex. The translation process is simplified to 3 steps: ribosome binding, translation, and termination. The concentration of ribosomes bound at the initiation site is $[ribo_{init}]$ and the concentration of translating ribosomes is $[ribo_{trans}]$ so that:

$$\begin{aligned} \frac{d[ribo_{init}]}{dt} &= k_{on}^{ribo} [RBS_{free}] [ribo_{free}] - k_{init}^{ribo} [ribo_{init}] \text{ and} \\ \frac{d[ribo_{trans}]}{dt} &= k_{init}^{ribo} [ribo_{init}] - k_{off}^{ribo} [ribo_{trans}], \end{aligned}$$

where free ribosomes, $[ribo_{free}]$, bind the initiation site, $[RBS_{free}]$, via mass action kinetics at a rate k_{on}^{ribo} . The rate of initiating translation is k_{init}^{ribo} and the termination rate is k_{off}^{ribo} .

In addition, we can write the total ribosome concentration, $[ribo_{total}]$, as the sum of the distinct pools of ribosomes so that

$$[ribo_{total}] = [ribo_{free}] + [ribo_{init}] + [ribo_{trans}].$$

Finally, we use the fact that the mRNA concentration equals to concentration of free ribosome binding sites (only one per mRNA) and the concentration of occupied ribosome binding sites:

$$[mRNA_{total}] = [ribo_{init}] + [RBS_{free}].$$

We then make the above equations dimensionless by scaling our variables. x denotes the translating ribosome fraction and y denotes the initiating ribosome fraction of total ribosome. The dimensionless equations are:

$$\frac{dx}{d\tau} = \gamma y - x$$

$$\frac{dy}{d\tau} = (\alpha - \beta y) (1 - x - y) - \gamma y.$$

where the dimensionless parameters are given by:

Parameters		
$\alpha = \frac{[mRNA]k_{on}^{ribo}}{k_{off}^{ribo}}$		Relative mRNA concentration
$\beta = \frac{[ribo_{total}]k_{on}^{ribo}}{k_{off}^{ribo}}$		Relative ribosome concentration
$\gamma = \frac{k_{init}^{ribo}}{k_{off}^{ribo}}$		Relative initiation rate
$\tau = t \times k_{off}^{ribo}$		Dimensionless time

At steady-state:

$$\gamma y - x = 0,$$

$$(\alpha - \beta y) (1 - x - y) - \gamma y = 0.$$

Thus, we have $x_{ss} = \gamma y_{ss}$. Replacing the above equation gives

$$(\alpha - \beta y) (1 - \gamma y - y) - \gamma y = 0,$$

Which can be rewritten as

$$(\gamma\beta + \beta)y^2 - (\beta + \alpha\gamma + \alpha + \gamma)y + \alpha = 0.$$

We note that α , β and $\gamma > 0$, and the translating ribosome fraction should also be positive. The above equation can then be solved to calculate the translating ribosome fraction y as a function of the relative mRNA and ribosome concentrations, α and β , respectively, so that:

$$y = \frac{\alpha + \beta + \gamma + \alpha\gamma - \sqrt{(\alpha + \beta + \gamma + \alpha\gamma)^2 - 4\alpha\beta(\gamma + 1)}}{2\beta(\gamma + 1)}.$$

We define the active ribosome fraction $\phi_a = x + y$ so that the above equation can be rearranged to yield:

$$\phi_a = \frac{\alpha + \beta + \gamma + \alpha\gamma - \sqrt{(\alpha + \beta + \gamma + \alpha\gamma)^2 - 4\alpha\beta(\gamma + 1)}}{2\beta}.$$

We next evaluate three dimensionless parameters as follows. Yeast cells typically contain ~60,000 mRNA transcripts^{31,64} and ~180,000-300,000 ribosomes^{32,64} in glucose, so that the ribosome-to-mRNA ratio $\beta_{glc}/\alpha_{glc} \sim 3$. We use a linear fit to our data to determine the relationship between both ribosome and mRNA concentrations and the growth rate so that the ribosome-to-mRNA ratios β/α at different growth rates can be calculated. γ , the initiation rate-to-termination rate ratio can be estimated from the number of initiating and elongating ribosomes. Approximately 4% of bound ribosomes (2% in polysomes, 7% in monosomes) are engaged in initiation in glucose²⁶, thus we

set $\frac{x_{glc}}{y_{glc}} = \gamma_{glc} = 24$. Our results show that the elongation rate remains constant across the tested carbon sources. Here, we assume the initiation rate is also constant and infer

an initiation-to-termination ratio (γ) of about 24 in all conditions. Then, the active ribosome fraction is a function of the growth rate with only one free parameter α_{glc} , whose best fit value is 2.05 (least squares fit). After determining the fraction of active ribosomes from mRNA and ribosome concentrations, the cellular growth rate can be estimated using the method described in the section “Estimate average peptide elongation rate of active ribosomes”, setting the peptide elongation rate to 9 amino acids per second.

G1 arrest experiment

G1 arrest time-course experiments were done using SCGE media. These strains lack the endogenous G1 cyclins (*cln1Δcln2Δcln3Δ*) require β -estradiol (BE) to express *CLN1* from a synthetic promoter. When this strain was proliferating, we used a concentration of 20 nM BE (Sigma-Aldrich, cat. no. E2758). To trigger the arrest, cells were washed and resuspended in pre-warmed medium lacking BE at $t = 0$ minutes. We measure the growth rate by both Beckman Z2 Coulter counter and spectrophotometer every 20 min. At t minutes, the local growth rate was determined by calculating the slope of the cell size/OD versus time using measurements taken at five points: $t-40$ min, $t-20$ min, t , $t+20$ min, and $t+40$ min. The average of local growth rates measured by OD600 and cell size are presented as data.

To estimate the active ribosome fraction and growth rate in **Fig. 4g**, we introduced mRNA concentration data in SCGE after G1 cyclin shut-off from Swaffer et al.²⁵, where the mRNA concentration in SCGE before arrest is estimated as 0.42 relative to glucose. Since the total ribosome content after G1 arrest is constant⁵⁴, we set ribosome content as 15.5% of the proteome as determined in **Fig. 1a**.

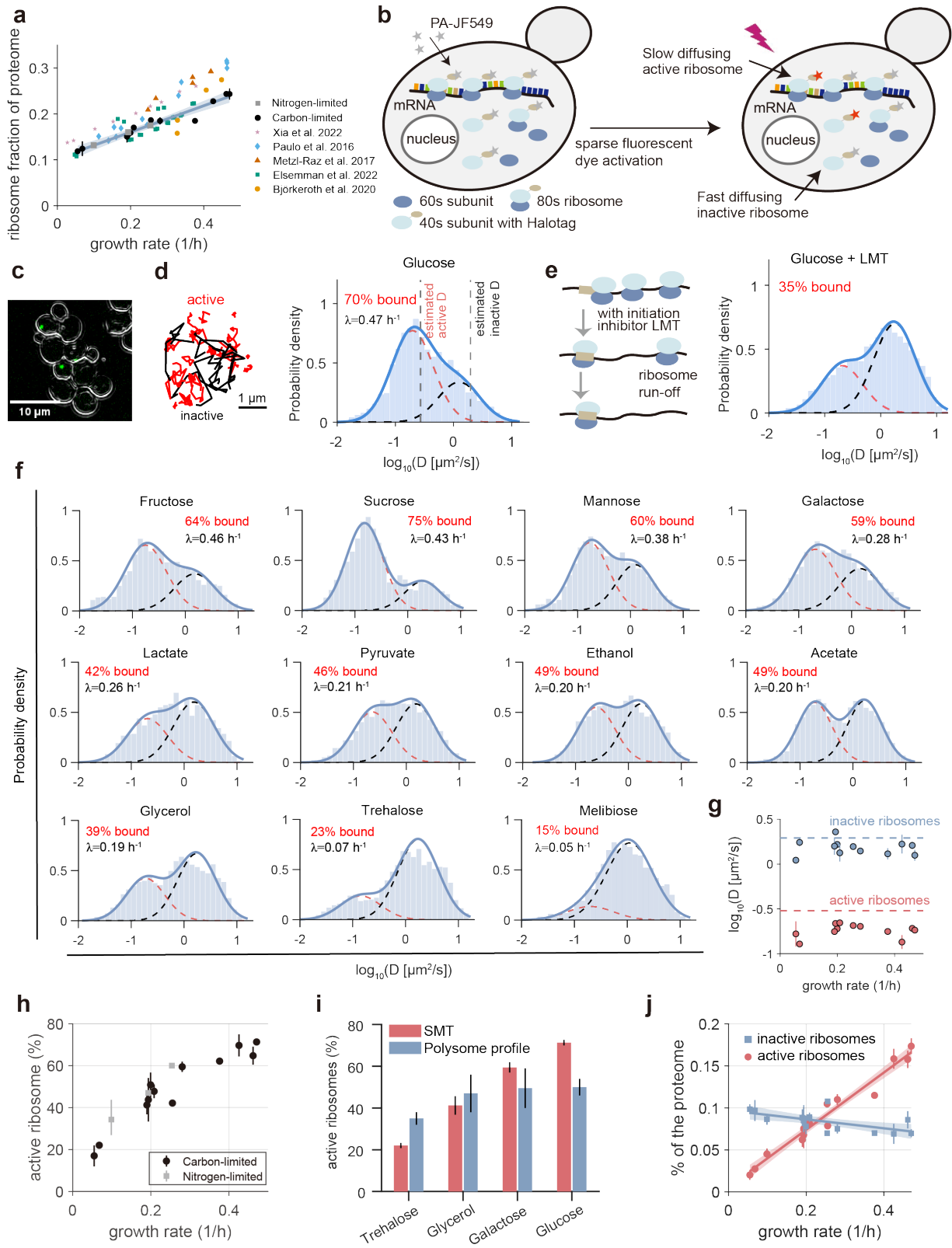


Figure 1: Quantification of active ribosome fraction using single-molecule tracking (SMT).

a, Total ribosome fraction of the proteome increases with growth rate. Black dots are our data, while colored dots are data from previous studies³⁻⁷. The blue line is the best-fit linear regression with 99% confidence interval (CI). Data are presented as mean \pm SEM (n = 3 for glucose; n = 2 for galactose, glycerol, and trehalose).

b, Schematic diagram illustrating single-molecule tracking of ribosomes. Active ribosomes bound to mRNA exhibit slower diffusion compared to free, inactive ribosomes.

c, Composite bright-field and fluorescence single-molecule tracking image. Green dots indicate individual active ribosomes.

d, Left: Representative trajectories of active (red) and inactive (black) ribosomes as measured by single-molecule tracking. Right: The fractions of active and inactive ribosomes were distinguished using a Gaussian mixture model. Distribution of ribosomal diffusion coefficients in yeast cultured in glucose (n = 4,091 tracks). Gray dotted lines indicate theoretical estimates of the diffusion coefficients of active and inactive ribosomes.

e, Left: Schematic depicting lactimidomycin (LMT) treatment, which inhibits ribosomes at the translation initiation site. Right: Distribution of ribosomal diffusion coefficients following 4 μ M LMT treatment (n = 5,532 tracks).

f, Distributions of ribosomal diffusion coefficients across yeast cultured in SC media with fructose (n=1,916 tracks), sucrose (n=2,376 tracks), mannose (n=3,730 tracks), acetate (n=2,790 tracks), galactose (n=4,679 tracks), lactate (n=2,269 tracks), ethanol (n=4,231 tracks), pyruvate (n=2,479 tracks), glycerol (n=2,548 tracks), trehalose (n=3,351 tracks), and melibiose (n=3,722 tracks).

g, Average diffusion coefficient of active (red) and inactive (blue) ribosomes in 12 carbon-limited conditions. Dotted lines indicate the predicted diffusion coefficients, as described in Fig. 1d.

h, The fraction of active ribosomes increases with growth rate. Black dots represent carbon-limited conditions, while gray dots represent nitrogen-limited conditions. The fraction of active ribosomes is shown as mean \pm range (n=2), while growth rate is shown as the mean of three biological replicates (n=3).

i, Comparison of the fraction of active ribosomes measured by single-molecule tracking (red) and polysome profiling (blue) across four conditions. Data are mean \pm range (n = 2).

j, Variation of active and inactive ribosome fractions of the proteome with growth rate. Active ribosome content was calculated as the product of total ribosome content and the active ribosome fraction. Data are presented as mean \pm SEM (from error propagation). Red and blue lines represent linear fits of active and inactive ribosome content, respectively. Shaded areas indicate the 90% CI.

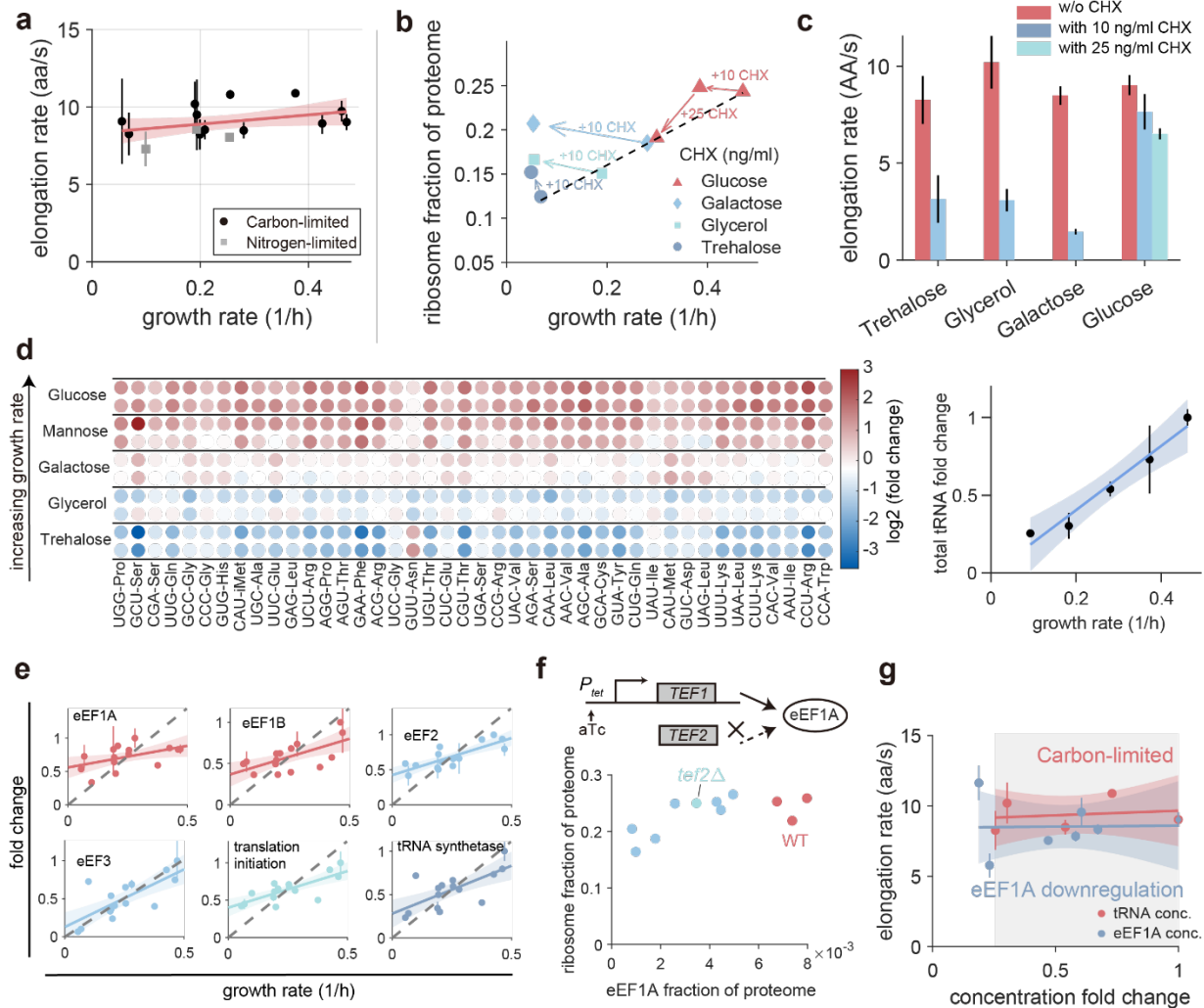


Figure 2: Buffered tRNA maintains a constant peptide elongation rate across different growth conditions

a, Peptide elongation rates calculated for cells growing on 12 different carbon sources. The red line represents a linear fit with a 90% confidence interval. Data are shown as mean \pm SEM (from error propagation).

b, Variation in ribosome content following treatment with the translation inhibitor cycloheximide (CHX) across four carbon sources. Colors indicate different carbon sources and arrows represent changes in ribosome content upon CHX treatment. The black dashed line shows a linear fit of ribosome content without CHX.

c, Peptide elongation rates calculated for cells growing on four carbon sources following CHX treatment. Gray bars represent elongation rates without CHX treatment for comparison. Data are shown as mean \pm SEM (from error propagation).

d, The heatmap shows the \log_2 fold changes of all 42 tRNA concentrations measured by RT-qPCR. Values of each tRNA were normalized to the mean tRNA levels across the five carbon sources. The right panel displays the total tRNA concentration fold changes across these conditions. Data show the mean with range (n=2).

e, Fraction of the proteome plotted against growth rate for elongation factor eEF1A, eEF1B, eEF2, eEF3, tRNA synthetase, and all initiation factors added together (**Supplementary Table 2; Extended Data Fig. 4c**). Solid lines indicate linear fits with 90% CI. The dashed black line denotes proportional scaling with growth rate. Data are presented as mean \pm range (n = 3 for glucose; n = 2 for galactose, glycerol, and trehalose) and normalized to the maximal value.

f, Schematic diagram of exogenously controlled eEF1A protein expression. The *TEF2* gene was deleted, and the promoter of *TEF1* was replaced with an anhydrotetracycline (aTc)-inducible P_{tet} promoter. The bottom panel shows ribosome content at different eEF1A expression levels.

g, Red dots show the peptide elongation rate remains nearly constant across different carbon sources despite changes to the total tRNA concentration. Blue dots show the peptide elongation rate as a function of eEF1A expression levels in the P_{tet} -*TEF1* system (mean \pm SEM, estimated by error propagation). Solid lines are linear fit with 90% confidence intervals, and the gray shaded area indicates the range in which tRNA is buffered.

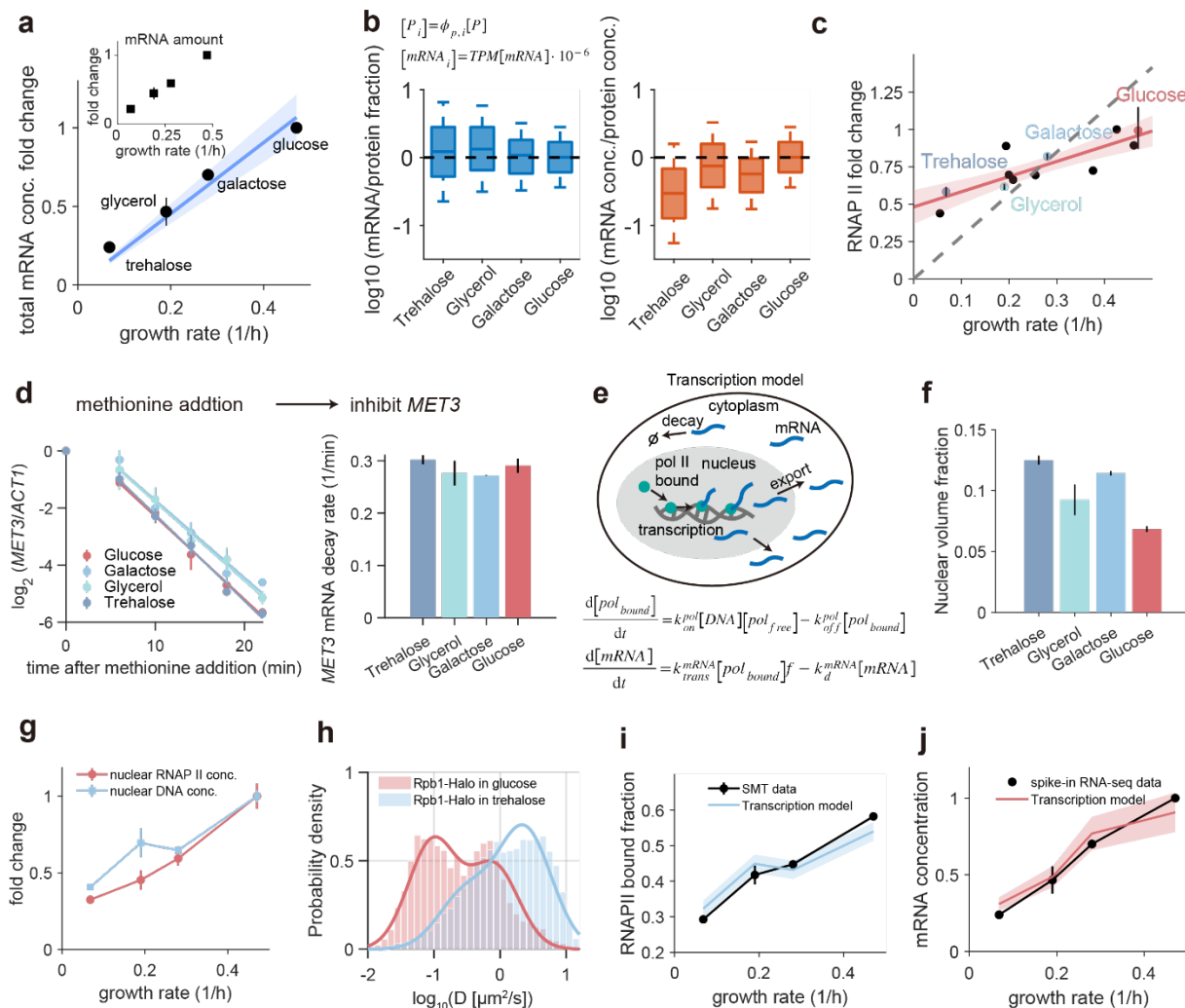


Figure 3: RNAPII kinetics scale total mRNA concentration with growth rate

a, mRNA concentration measured by spike-in mRNA sequencing in four conditions (see **Extended Data Fig. 5b**). Data are mean with SEM (estimated from error propagation).

The blue line denotes the linear fit of mRNA concentration with 90% CI. The inset shows the corresponding changes in mRNA amount.

b, Left: Median with interquartile range (IQR) of the mRNA fraction-to-protein fraction ratio for 1,795 genes across four growth conditions. Right: Median with IQR of mRNA concentration-to-protein concentration of 1,795 genes across four growth conditions. The individual protein concentrations were calculated by multiplying its protein fraction by the total protein concentration. The mRNA fraction for each gene is its TPM value divided by 10^6 . mRNA concentrations were calculated as the product of the mRNA fraction and total mRNA concentration.

c, RNAP II protein expression level across 12 different carbon sources, where four conditions were highlighted in which mRNA concentration was also measured. The shaded area denotes the 90% CI of a linear fit. Data are presented as mean \pm range (n = 3 for glucose; n = 2 for galactose, glycerol, and trehalose).

d, Left: *MET3* mRNA concentrations relative to *ACT1* mRNA after methionine addition represses *MET3* transcription in cells growing using 4 different carbon sources. Right: Mean (\pm range) of *MET3* mRNA decay rates measured in two biological replicates.

e, Schematic diagram showing transcription driven by mass action kinetics of RNAP II and the genome.

f, Nuclear fraction of cell volumes measured by Pus1-eGFP fluorescent nuclear protein in four conditions. Data are presented as mean with range from two biological replicates (see **Extended Data Fig. 6e**).

g, Nuclear RNAP II and DNA concentrations in the indicated conditions. Data are mean with SEM (from error propagation).

h, Histogram of the diffusion coefficient of Rpb1, determined from single-molecule tracking, for *RPB1-Halo* in glucose (n = 3,930 tracks) and *RPB1-Halo* in trehalose (n=12,776 tracks).

i, The fraction of DNA-bound Rpb1 molecules as a function of growth rate. Data (black dots) are shown as the mean with range, n=2. The bound fraction of RNAPII is predicted by our transcription model. The shaded area indicates the 90% confidence interval of the model estimate.

j, Predicted mRNA concentration changes from our transcription model. The shaded area indicates the 90% confidence intervals of the model estimate.

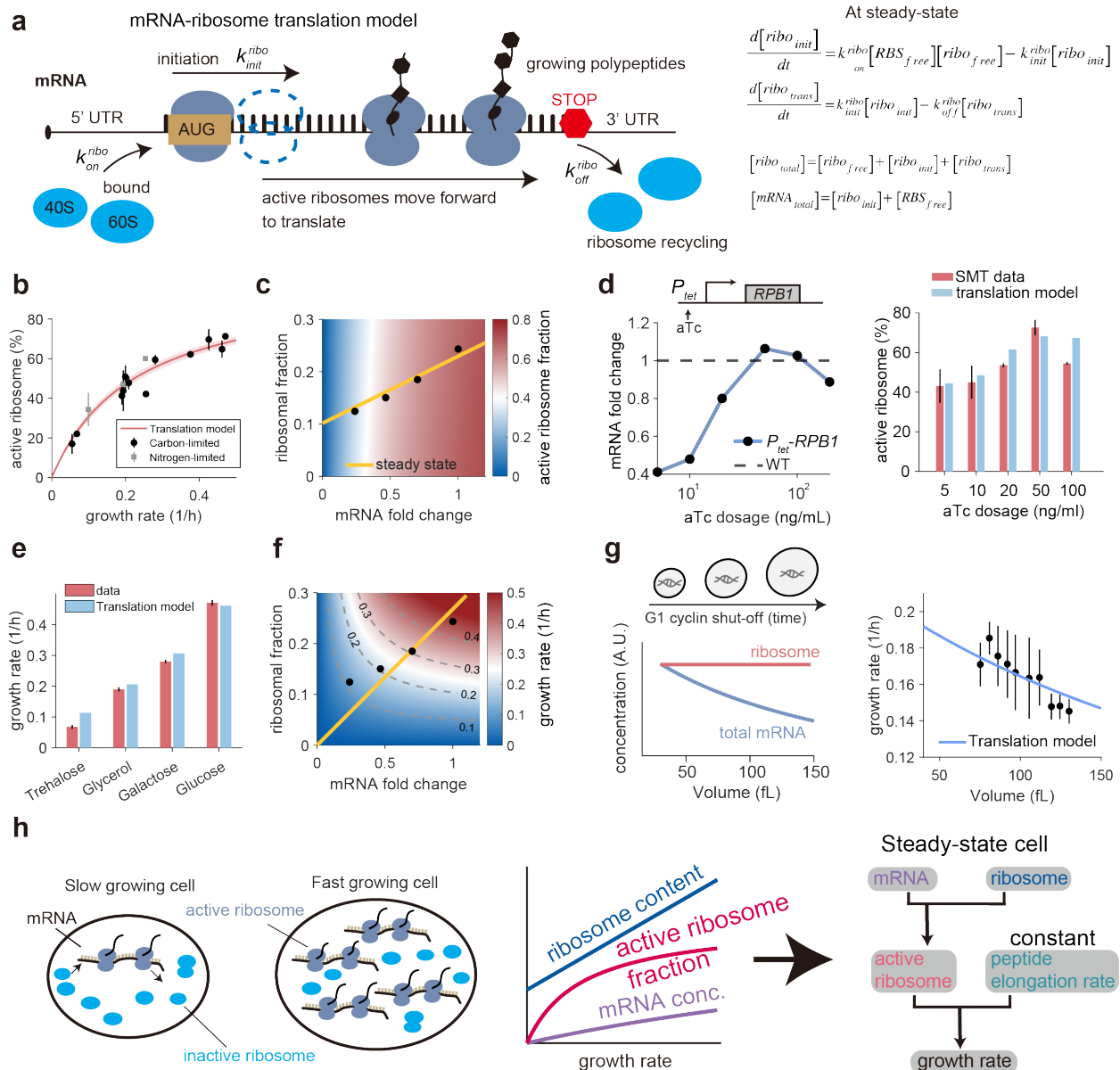


Figure 4: mRNA and ribosome mass action kinetics determine the active ribosome fraction and growth rate.

a, Schematic illustrating the mRNA–ribosome mass action kinetic model for protein translation.

b, The fraction of active ribosomes were fit using our translation model. The shaded area represents the 90% confidence interval of the single parameter model fit. Experimental data are from Fig. 1h.

c, Heatmap showing how relative mRNA and ribosome concentrations affect the fraction of active ribosomes (color scale). Data points represent measurements from

four growth conditions. The yellow line indicates the coordinated adjustment of mRNA and ribosome levels with increasing growth rates.

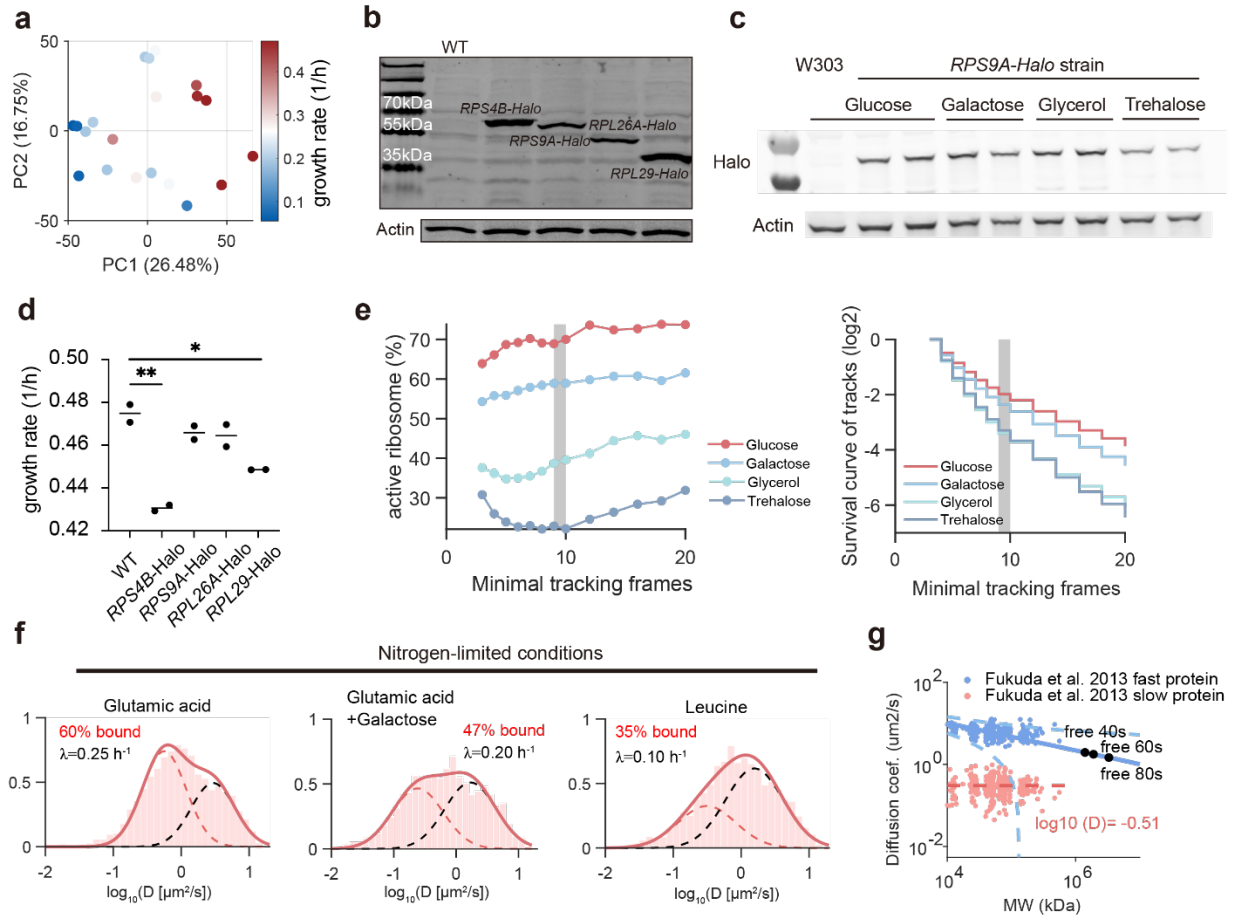
d, Left: The fold change of mRNA concentration of the $P_{tet}\text{-}RPB1$ strain at the indicated aTc concentrations. mRNA concentrations were quantified by spike-in RNA sequencing. The dashed line indicates the total mRNA concentration of the wild-type strain grown in glucose. Right panel: The fraction of active ribosomes in the $P_{tet}\text{-}RPB1$ strain with different aTc concentrations, measured by single-molecule tracking (SMT). Data are shown as mean \pm SEM ($n = 3$ for 5 and 10 ng/mL aTc; $n = 2$ for all others) and compared with the predicted values of our translation model.

e, The growth rates in four conditions (mean with SEM, $n=3$) were compared with model results, which are calculated from the translation model taking the mRNA and ribosome concentrations as input.

f, Heatmap showing the effect of relative mRNA and ribosome concentrations on growth rate. Gray contour lines indicate equal growth rate. The yellow solid line indicates proportional increases of mRNA and ribosome concentrations.

g, Left panel: Schematic indicating G1 arrested yeast cells growing larger to dilute the genome and dilute mRNA while the ribosome concentration remains constant. Right: Comparison of the predicted and measured growth rates for these cells. Data show mean values with SEM ($n=4$).

h, Schematic diagram illustrates how cell growth is organized in fast and slow growth conditions.



Extended Data Fig. 1: Quantification of active ribosome fraction by single-molecule tracking (SMT), related to Fig. 1.

a, Principle component analysis of proteomic data for yeast grown on the indicated carbon sources. Color denotes the growth rate.

b, Immunoblot analysis confirms successful incorporation of a Halo tag into the ribosomal proteins Rps4B, Rps9A, Rpl26A, and Rpl29 in the 4 indicated strains.

c, Immunoblot showing the expression of the Halo tag in an *RPS9A-Halo* strain in the indicated SC media.

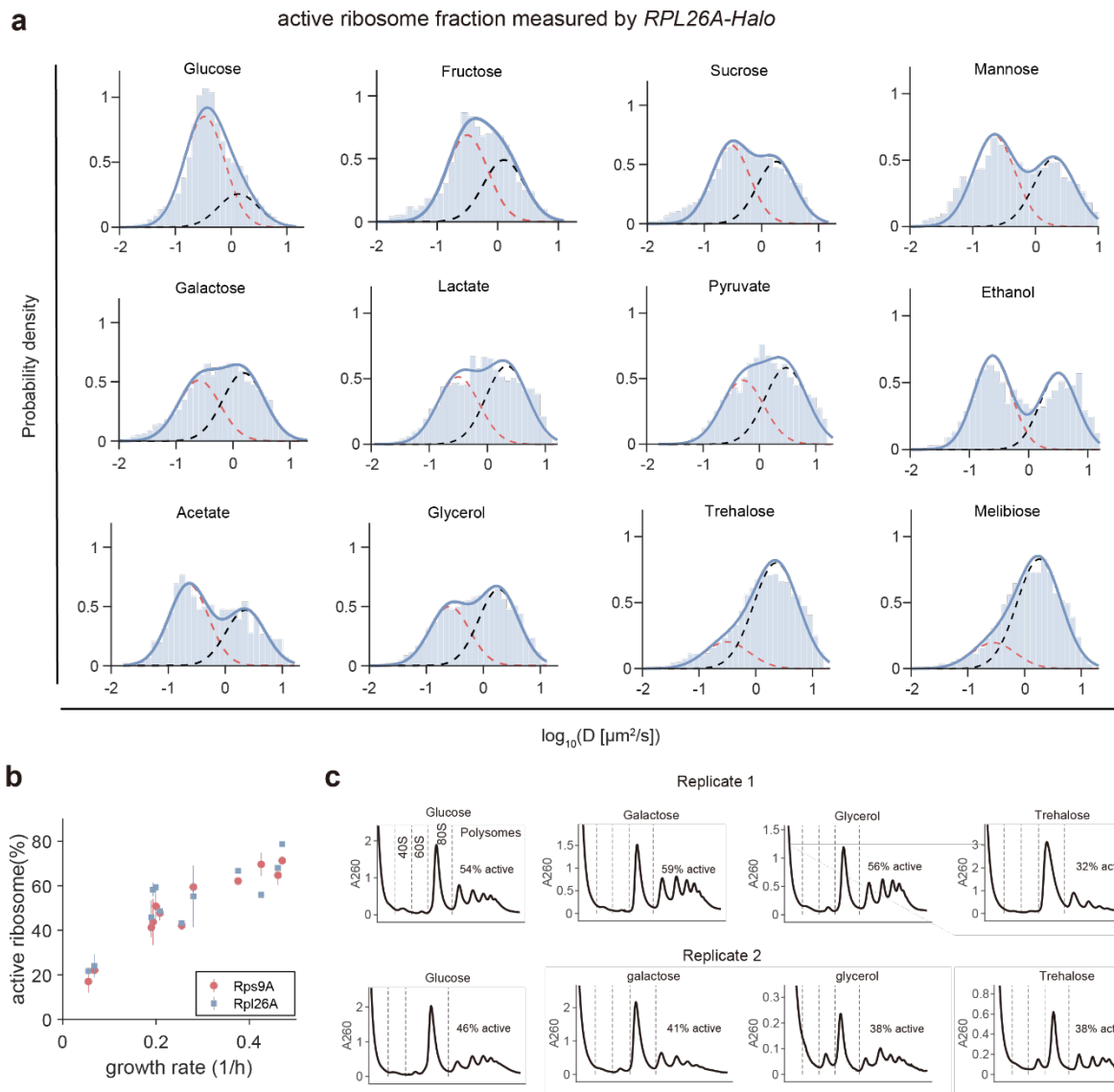
d, Growth rates for the indicated strains in SCD media. * denotes $p < 0.05$ and ** denotes $p < 0.01$ calculated using an unpaired t-test was performed.

e, Left: The active ribosome fraction calculated by different minimum numbers of single molecule tracking frames. Right: Fraction of molecules tracked for more than the indicated number of frames. Measurements based on trajectories lasting at least 9 frames (shaded region) provided robust results balancing the trade off of getting more frames with the loss of molecules during tracking.

f, Distributions of ribosomal diffusion coefficients for yeast cultured in nitrogen-limited conditions with glutamic acid (n=5,091 tracks), leucine (n=3,853 tracks) and glutamic acid+galactose combination (n=3,422 tracks).

g, Diffusion coefficient of free ribosome (D) can be estimated using the Stokes-Einstein

equation and is a function of molecular weight (MW) $D_i \sim k \times MW_i^{-\frac{1}{3}}$. The active ribosome diffusion coefficient was approximated from average values of other slow-moving proteins.

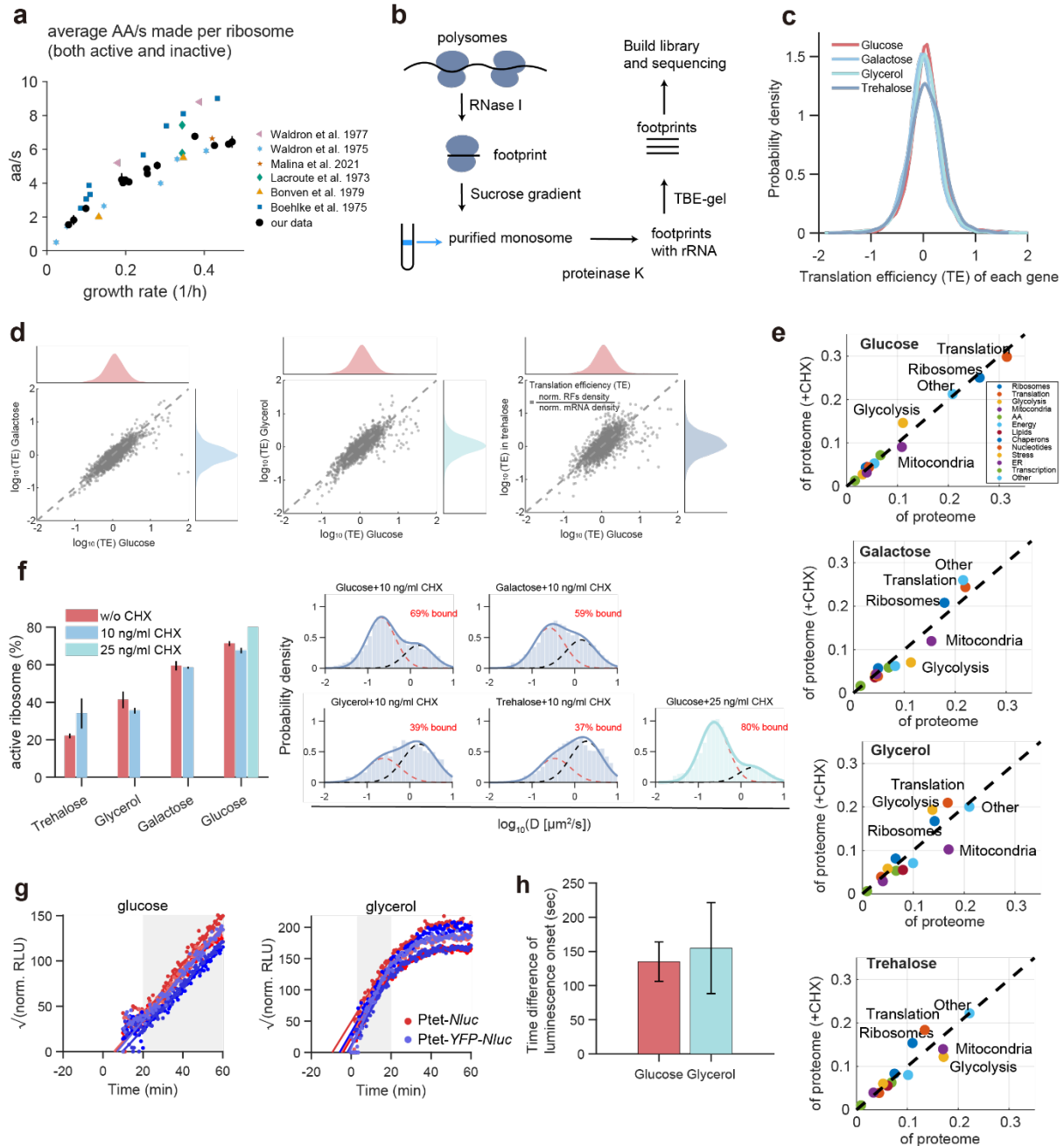


Extended Data Fig. 2: Active ribosome fraction measured using *RPL26A-Halo* to tag the large subunit, related to Fig. 1.

a, Diffusion coefficient distributions were determined using *RPL26A-Halo* for cells grown on indicated carbon sources. The number of tracks analyzed was $n = 11,209$ for glucose, $n = 5,075$ for fructose, $n = 12,061$ for sucrose, $n = 1,806$ for mannose, $n = 1,078$ for acetate, $n = 6,008$ for galactose, $n = 2,306$ for lactate, $n = 2,443$ for ethanol, $n = 2,643$ for pyruvate, $n = 5,942$ for trehalose, and $n = 8,552$ for melibiose.

b, Comparison of active ribosome fractions measured by tagging Rps9A (40S subunit) and Rpl26A (60S subunit) with Halo tags. Data are presented as mean with range ($n=2$).

c, Polysome profiling results for yeast cells cultured in SC medium with glucose, galactose, glycerol, and trehalose (n=2). Peaks corresponding to 40S, 60S, monosomes, and polysomes are indicated.



Extended Data Fig. 3: Translation machinery and rate analysis, related to Fig. 2.

a, Under the assumption that all ribosomes are active, the average elongation rate of total ribosomes is shown to monotonically increase with the growth rate. Colored dots indicate data from previous studies^{15,16,18–20,41}. Data are presented as mean \pm SEM (from error propagation).

b, Workflow schematic illustrating the procedure for ribosome footprint sequencing.

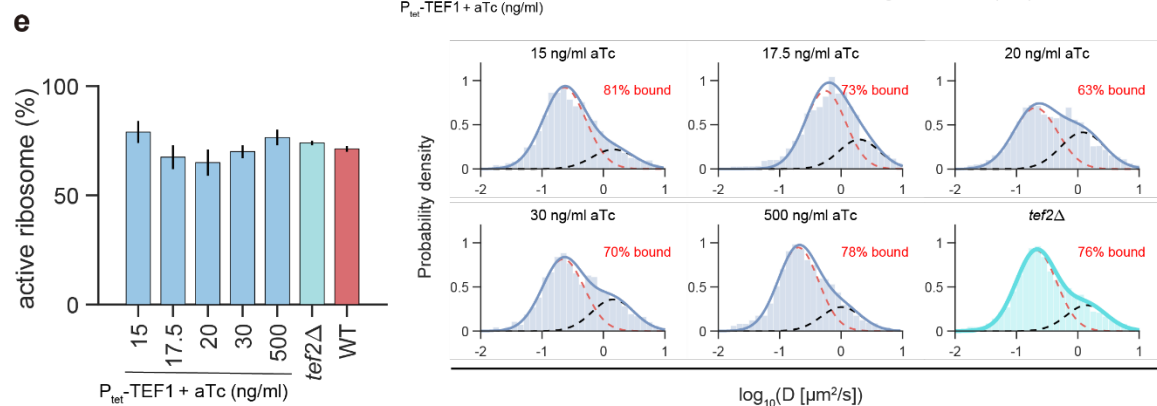
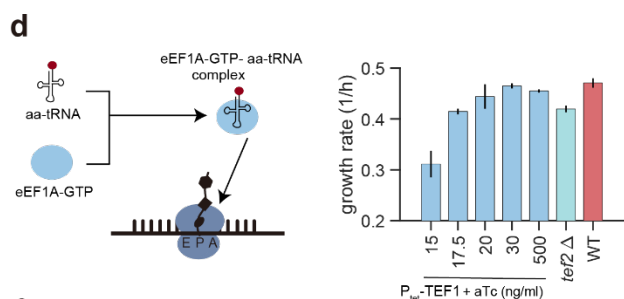
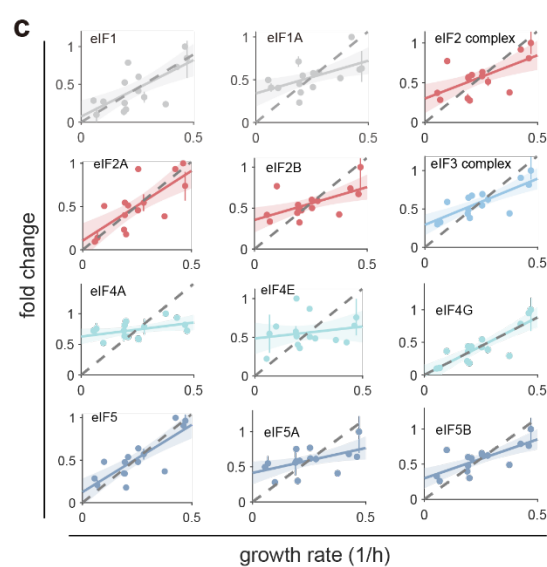
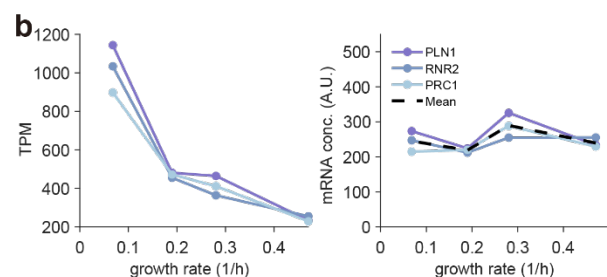
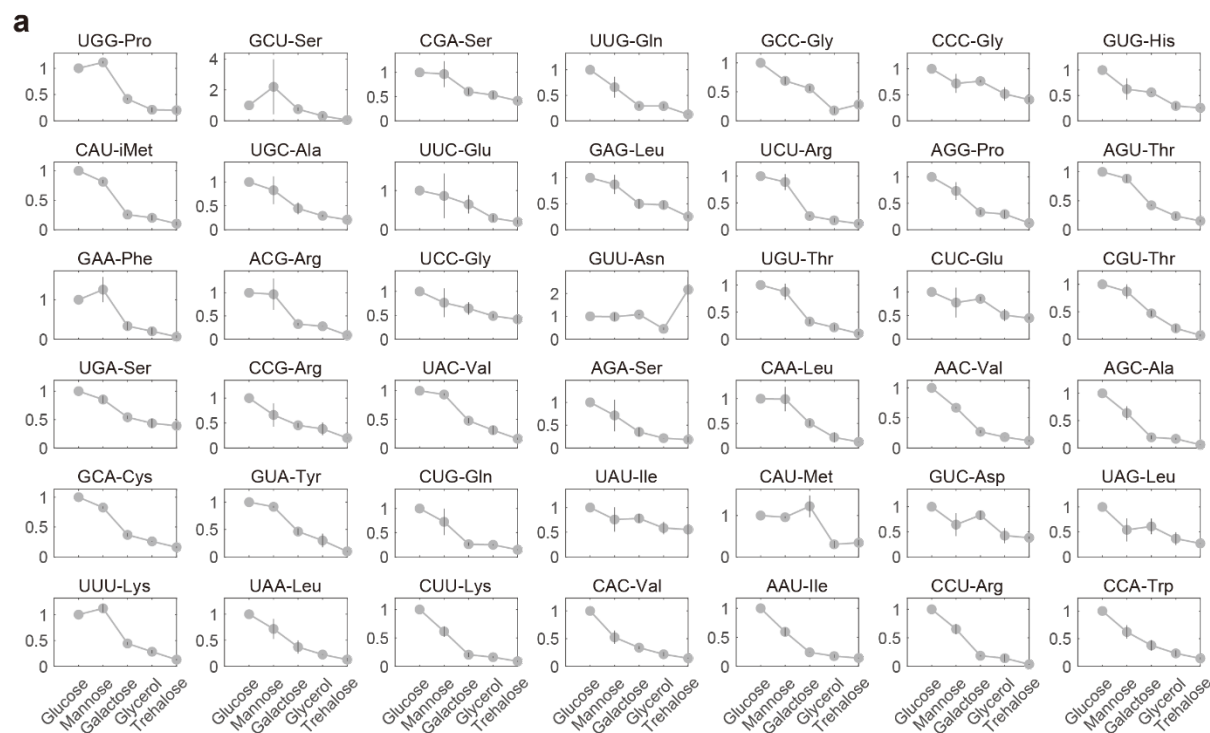
c-d, Translation efficiency (TE) of 2,055 genes under the 4 indicated growth conditions. TE is defined as normalized ribosome footprint density divided by normalized mRNA density (see **Methods**). Marginal distributions show the TE distribution under each carbon source.

e, Comparison of overall proteome composition after CHX treatment in four carbon sources. The proteomic classification follows categories defined by previous work⁴.

f, Distributions of ribosomal diffusion coefficients determine the active ribosome fraction in SC media with glucose (n = 12,079 tracks), galactose (n = 5,153 tracks), glycerol (n = 3,018 tracks), and trehalose (n = 4,407 tracks) with and without CHX treatment.

g, Luminescence was measured over time after aTc induction in two reporter constructs: P_{tet} -Nluc and P_{tet} -YFP-Nluc. The square root of normalized relative luminescence units (RLU) was plotted to estimate translation onset (see **Methods**). Linear fits within the shaded region were used to extrapolate the time of first detectable luminescence. Three biological replicates were performed for each condition.

h, Time differences of P_{tet} -Nluc and P_{tet} -YFP-Nluc luminescence onset between glucose and glycerol conditions. Error bars represent the SEM of the time difference between YFP-Nluc and Nluc onset, calculated from the 3×3 pairwise comparisons (n = 9).



Extended Data Fig. 4: Analysis of tRNA concentrations and eEF1A downregulation, related to Fig. 2.

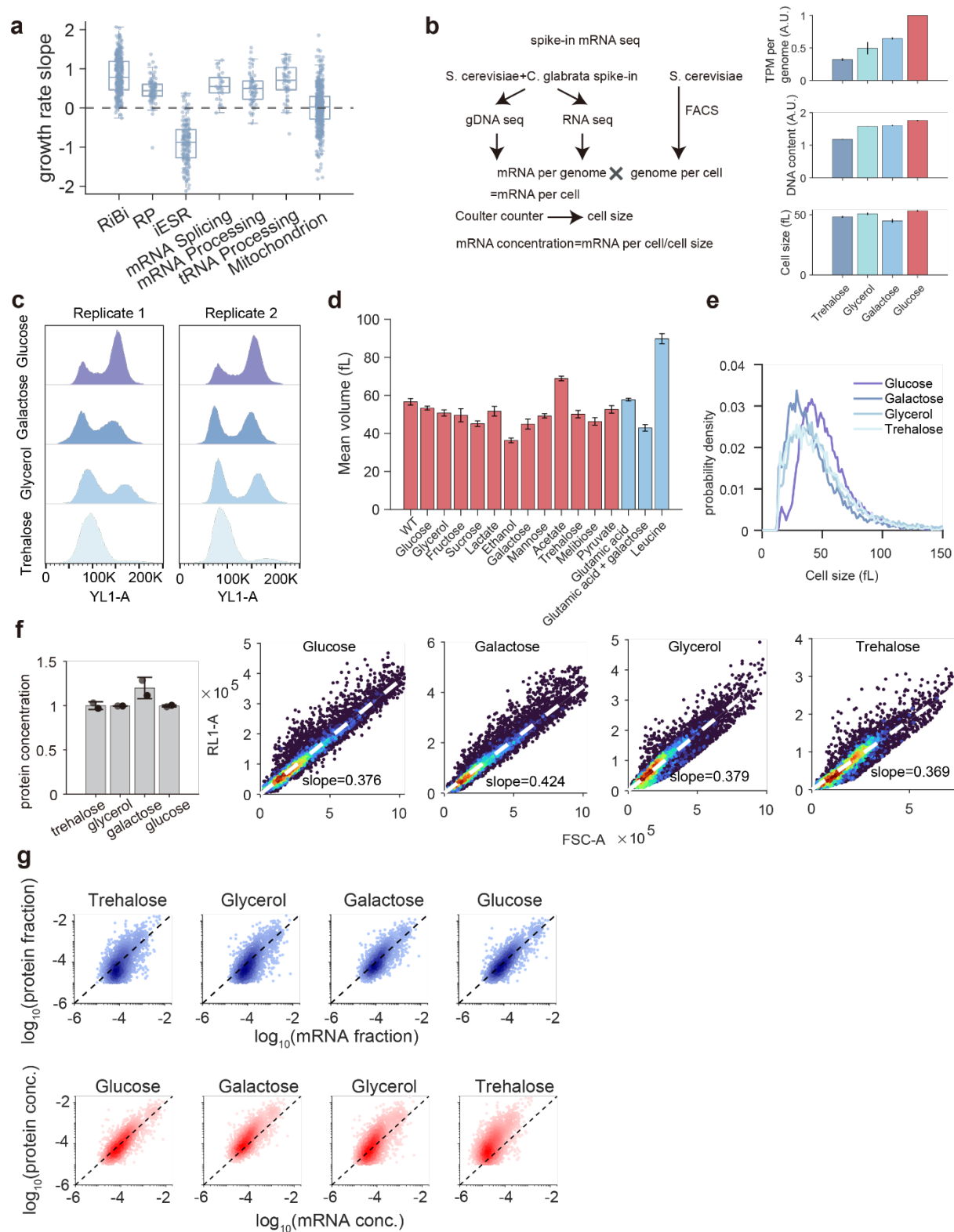
a, Fold changes in concentration of all 42 tRNA species across the indicated conditions are shown. Data represent the mean and range (n = 2).

b, Expression analysis of housekeeping genes *PLN1*, *RNR2*, and *PRC1*. Transcripts per million (TPM, left panel) decrease slightly with increasing growth rate, while their mRNA concentrations remain largely constant across conditions. The relative mRNA concentration of a given gene is calculated as TPM multiplied by the global mRNA concentration (see **Fig. 3a**).

c, Fraction of the proteome plotted against growth rate for initiation factor eIF1, eEF1A, eIF2, eIF2A, eIF2B, eIF3, eIF4A, eIF4E, eIF4G, eIF5, eIF5A, and eIF5B. Solid lines indicate linear fits with 90% CI. The dashed black line denotes proportional scaling with growth rate. Data are presented as mean \pm range (n = 3 for glucose; n = 2 for galactose, glycerol, and trehalose) and normalized to the maximal value.

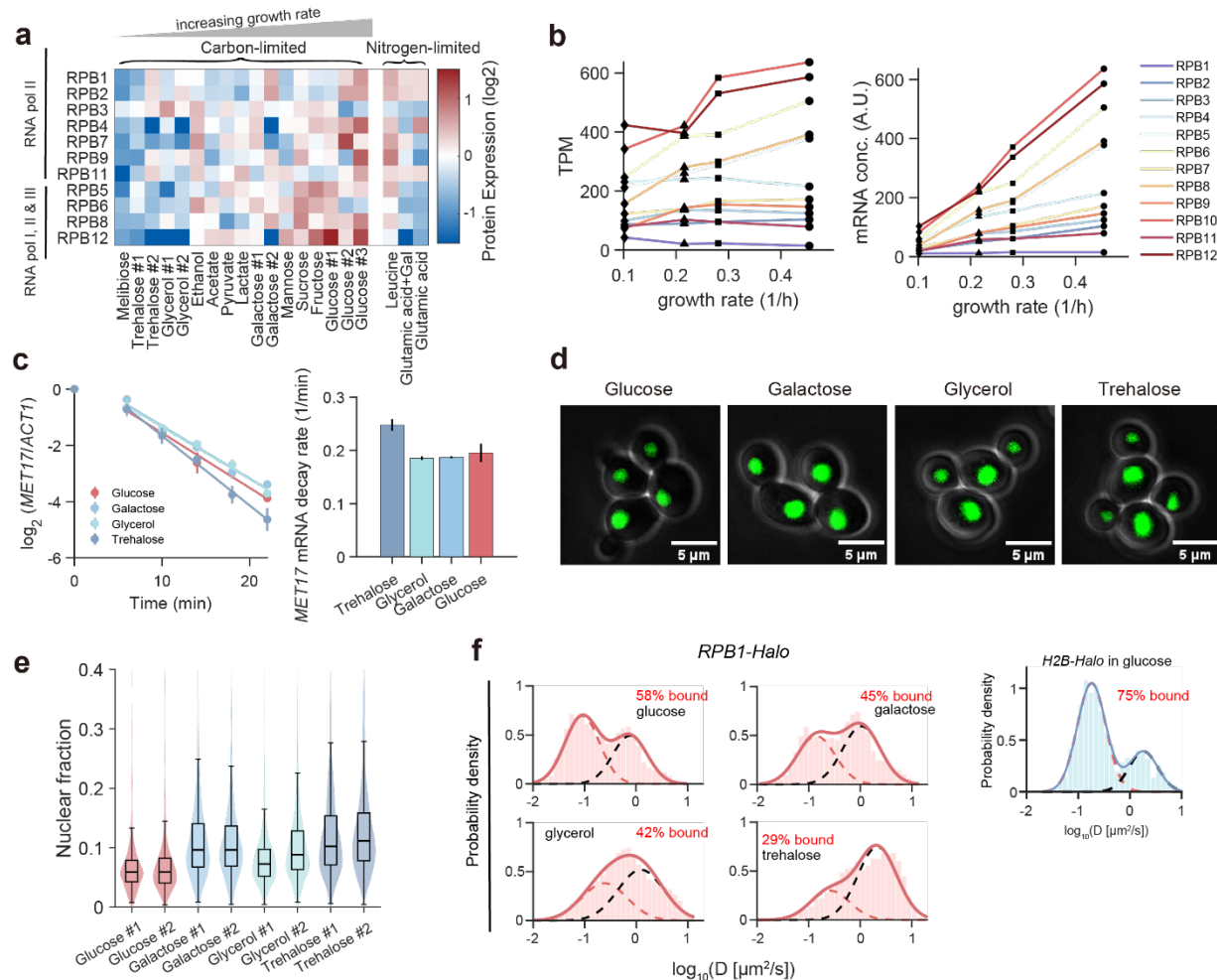
d, The growth rates are shown for the *P_{tet}-TEF1 tef2 Δ* strain treated with different aTc concentrations, the *tef2 Δ* strain, and a wild type strain. Data are mean with SEM (n=3).

e, The fraction of active ribosomes are shown for the *P_{tet}-TEF1 tef2 Δ* strain treated with different aTc concentrations, the *tef2 Δ* strain, and a wild type strain. Data indicate the mean and range (n=2). For the diffusion tracks: n=2,867 with 15 ng/ml aTc; n=2,268 with 17.5 ng/ml aTc; n=4,342 with 20 ng/ml aTc; n=2,365 with 30 ng/ml aTc; n=2,814 with 500 ng/ml aTc; n=3273 in the *tef2 Δ* strain.



Extended Data Fig. 5: Spike-in RNA sequencing to determine global mRNA concentrations, related to Fig.3.

- a**, The box plot illustrates the slopes of protein abundance versus growth rate for ribosome biogenesis (RiBi), ribosomal proteins (RP), induced environmental stress response (iESR), mRNA splicing, mRNA processing, tRNA processing, and mitochondrion. Each box shows the median and interquartile range (IQR). The classification of these proteins is provided in **Supplementary Table 2**.
- b**, Workflow schematic of spike-in RNA sequencing to quantify global mRNA concentration. Right: normalized TPM per genome (n=2), average DNA content per cell (n=2), and average cell volume (n=3) measured under these four conditions. These parameters were used to calculate the global mRNA concentration. Data are mean with SEM.
- c**, Flow cytometry data showing DNA content distributions in cells cultured in SC media with four different carbon sources.
- d**, Average cell volume (mean \pm SD, n=3) for yeast populations cultured in SC media with 12 different carbon sources and 3 nitrogen sources.
- e**, Characteristic cell size distributions from Coulter counter measurements of cells growing in the indicated conditions.
- f**, Global protein concentration measurements by flow cytometry. Cells were stained using NHS-ester dye, and protein levels were quantified from the slope of robust linear regression of fluorescence intensity against forward scatter (FSC-A) shown in the right hand panels. Data are presented as the mean and range (n = 2).
- g**, Correlation of protein and mRNA fractions and concentrations for 1,795 genes across four conditions with different growth rates.



Extended Data Fig. 6: Analysis of RNAP II activity, related to Fig. 3

a, Protein concentrations for the 12 RNA polymerase II subunits across 12 different carbon sources.

b, TPM and mRNA concentrations for the 12 RNA polymerase II subunits across 12 different carbon sources.

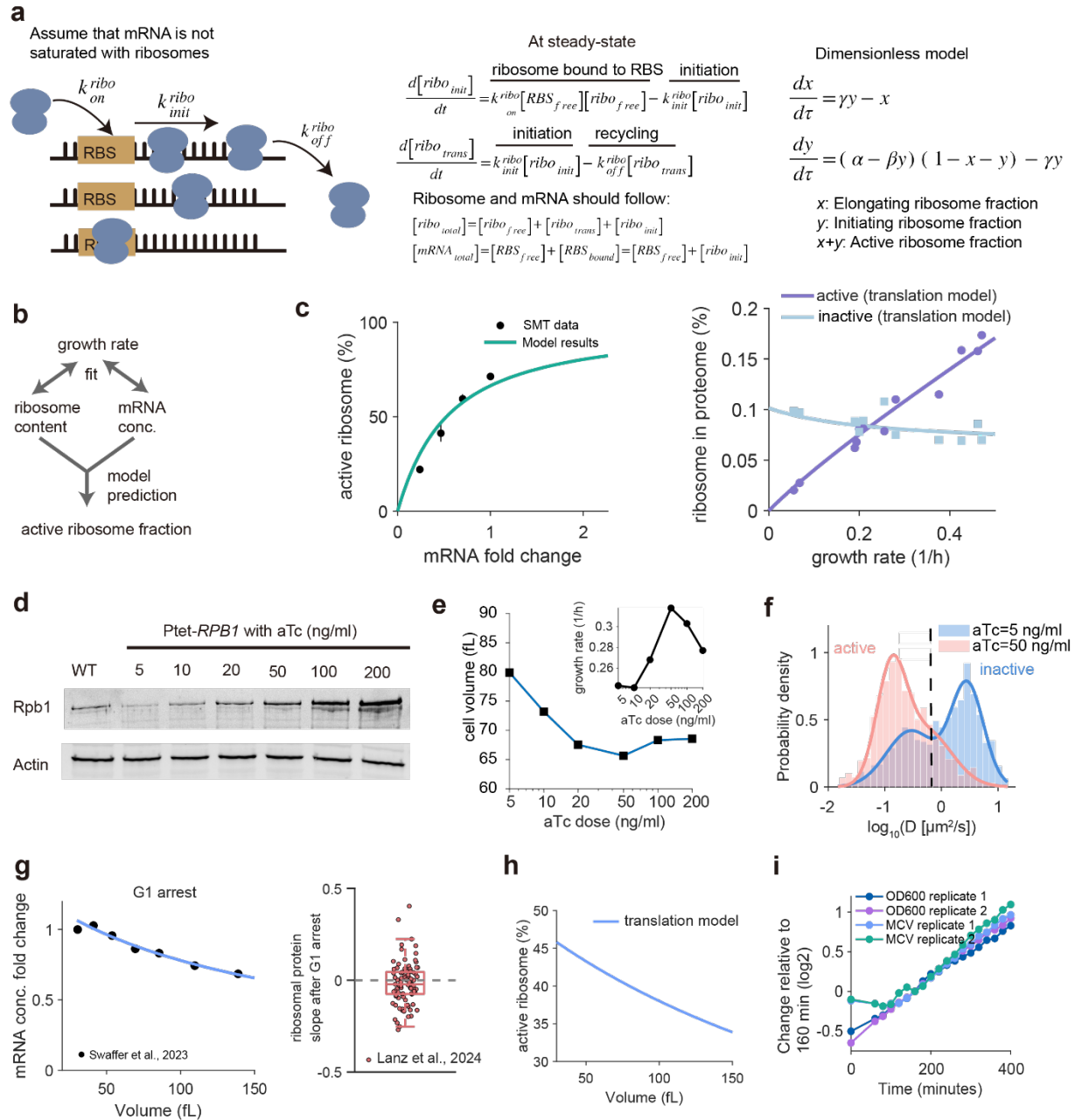
c, Left: *MET17* mRNA concentration relative to *ACT1* mRNA concentration after methionine addition to the media for cells growing in the indicated carbon sources. Right: mean (\pm range) *MET17* mRNA decay rates ($n = 2$).

d, Representative composite phase and fluorescence images of Pus1-eGFP expressing cells growing in SC media with the indicated carbon source.

e, Violin plots showing the distribution of nuclear volume fractions for cells growing in SC media with the indicated carbon sources ($n=687$ for glucose #1, $n=1,054$ for glucose #2, $n=503$ for galactose #1, $n=886$ for galactose #2, $n=475$ for glycerol #1, $n=1,286$ for

glycerol #2, n=515 for trehalose #1, and n=1,430 for trehalose #2). Each plot includes a box indicating the median and interquartile range.

f, Distribution of diffusion coefficients for RNAP II, where the Rpb1 subunit was tagged with Halo (n=2832 tracks in glucose, n=5392 tracks in galactose, n=4581 tracks in glycerol and n=8336 tracks in trehalose). Right: Distribution of diffusion coefficients for histones, where the histone 2 subunit H2B was tagged with Halo (n=1,237 tracks).



Extended Data Fig. 7: A dynamic equilibrium model for protein translation, related to Fig. 4.

a, Schematic illustrating the full dynamic equilibrium model, assuming ribosomes bind to mRNA without saturation. The system can be simplified into a dimensionless two-variable ordinary differential equation (ODE) model characterized by three parameters: relative mRNA concentration, relative ribosome concentration, and relative initiation rate (see **Methods**).

b, Workflow showing how we fit data to calculate the active ribosome fraction for each condition.

c, Comparison of data and the single parameter model fit predicting the fraction of active and inactive ribosomes.

d, Immunoblot showing Rpb1 protein expression at different aTc concentrations for a *P_{tet}-RPB1* strain.

e, Cell volume and growth rates at steady state for *P_{tet}-RPB1* cells growing in media with the indicated aTc concentration.

f, Distribution of ribosome diffusion coefficients in a *P_{tet}-RPB1* strain grown in media with 5 (n=1,785) and 50 ng/ml (n=1,490) aTc concentrations.

g, Left: After G1 arrest, the mRNA concentration decreases while cell volume increases. Data are from Swaffer et al ²⁵. Right: The slopes for fits of the normalized protein concentration versus normalized cell size for all the ribosomal protein subunits (for a detailed description of how these slopes were calculated, see Lanz et al ⁵⁴). A slope = 0 indicates a constant, size-independent concentration. Data are shown as median with IQR.

h, Dynamic equilibrium model prediction for the active ribosome fraction after G1 arrest.

i, OD600 and mean cell volume increase after G1 arrest. Data are normalized to values at 160 min. Measurements performed with two biological replicates.